



HAL
open science

Optimal combination of conventional MRI and DCE-MRI parameters to early predict pathologic response to anthracycline-based neoadjuvant chemotherapy for locally advanced high-grade soft-tissue sarcomas

Amandine Crombé

► **To cite this version:**

Amandine Crombé. Optimal combination of conventional MRI and DCE-MRI parameters to early predict pathologic response to anthracycline-based neoadjuvant chemotherapy for locally advanced high-grade soft-tissue sarcomas. Life Sciences [q-bio]. 2017. dumas-01649831

HAL Id: dumas-01649831

<https://dumas.ccsd.cnrs.fr/dumas-01649831>

Submitted on 27 Nov 2017

HAL is a multi-disciplinary open access archive for the deposit and dissemination of scientific research documents, whether they are published or not. The documents may come from teaching and research institutions in France or abroad, or from public or private research centers.

L'archive ouverte pluridisciplinaire **HAL**, est destinée au dépôt et à la diffusion de documents scientifiques de niveau recherche, publiés ou non, émanant des établissements d'enseignement et de recherche français ou étrangers, des laboratoires publics ou privés.

Université de Bordeaux

UFR DES SCIENCES MEDICALES

Année 2017

Thèse n° 3120

Thèse pour l'obtention du

DIPLOME D'ETAT DE DOCTEUR EN MEDECINE

Présentée et soutenue publiquement le 20 septembre 2017 par

Amandine CROMBE

Née le 11 Janvier 1985 à Paris 15^{ième}

Optimal combination of conventional MRI and DCE-MRI parameters to early predict pathologic response to anthracycline-based neoadjuvant chemotherapy for locally advanced high-grade soft-tissue sarcomas

DIRECTRICE DE THESE

Docteur Michèle KIND

MEMBRES DU JURY

Monsieur le Professeur Thomas TOURDIAS..... Président du jury
Monsieur le Professeur Antoine ITALIANO* Juge
Monsieur le Docteur François LE LOARER..... Juge
Monsieur le Docteur Eberhardt STOECKLE..... Juge
Monsieur le Docteur Nicolas ALBERTI..... Juge
Madame le Docteur Michèle KIND..... Juge
Monsieur le Professeur Jean-Michel COINDRE.....Juge

**absent le jour de la soutenance*

RAPPORTEUR

Professeur Nathalie LASSAU

ABSTRACT

Purpose : To determine which conventional MRI and Dynamic-contrast-enhanced MRI (DCE-MRI) qualitative, semi-quantitative, quantitative features are significantly associated with histologic response to anthracycline-based neoadjuvant chemotherapy (a-NAC) in locally advanced high grade soft-tissue sarcoma (STS). To estimate inter- and intra-observer agreements of each criterion.

Methods: Retrospective, monocentric exploratory study. 46 adults with biopsy-proven high-grade STS of trunk walls and extremities, uniformly treated in a French sarcoma reference centre with 5-6 cycles of a-NAC. Radiological evaluation consisted in conventional pre-therapeutic (t_0) MRI₀ and after 2-3 cycles of a-NAC (t_1) MRI₁+DCE-MRI₁. After 5-6 cycles of a-NAC (t_2), 32 patients also had MRI₂+DCE-MRI₂ for pre-operative evaluation. All had available pathological analysis of surgical specimen with treatment response estimation. Good or poor histologic response (GHR, PHR) was determined depending on % residual viable tumour cells ($\leq 10\%$ or $>10\%$, respectively). MRI were randomly analysed, two times by two radiologists, blinded to histological results. Conventional MRI lecture assessed tumour maximal size, bi-dimensional diameters, volume, as well as T1 and T2 signals, architecture, margins, oedema, nerve, vessels and bone invasion in a dichotomised fashion.

DCE-MRI was analysed on whole tumour surface (ROI_s) and on the first area displaying contrast uptake (ROI_N): qualitatively (%tumour volume enhanced during arterial phases, curvology), semi-quantitatively (model-free: wash-in (WIn), iAUC90, Peak-enhancement (PE), and their ratio versus healthy muscle) and quantitatively (extended Tofts model: K_{trans} and its ratio).

Se, Sp, PPV, OR were determined, as well as best cut-offs helped by receiver operating characteristics (ROC) curves analyses. Significant criteria to distinguish GHR and PHR at t_1 were used in a logistic binary regression to build a multivariate model to predict response. Inter- and intra-observer agreements were estimated.

At t_2 , correlation between %viable cells and numeric DCE-MRI₂ indices were evaluated with uni- and multivariate linear regression.

Results: 34 PHR and 12 GHR were included. Gender female was significantly associated with PHR ($p=0.015$). After 2-3 cycles of a-NAC, none of the change in measurements or on conventional MRI was significantly different between PHR and GHR. PE and WIn-ratio on ROI_N were significantly higher in PHR ($p=0.029$ and 0.048 , respectively). When gender, PE and WIn-ratios variables were considered together, they significantly predicted histologic response ($p=0.004$), but none individually reached significance. 94.1% PHR were well-classified. 45.5% GHR were ill-classified. AREA under ROC curve of the model was 0.846 IC_{95%}=[0.677-0.994].

At t_2 : %change of longest dimension, bi-dimensional diameter, volume since t_0 were significantly higher in GHR ($p=0.012, 0.010, 0.031$, respectively). WIn-ratio, PE, iAUC90, K_{trans} , K_{trans} -ratio in ROI_N ($p= 0.012, 0.010, 0.031, 0.022, 0.023, 0.020, 0,009, 0,010$, respectively) as well as K_{tran} , K_{trans} -ratio on ROI_s were lower in GHR ($p=0.043$ and 0.021 , respectively) . Multivariate linear regression analysis showed that WIn-ratio- $ROI_{n,2}$ and % change of the longest dimension were significantly correlated with % viable cells on following surgery ($r=0.370, p=0.022$ and $r=0.394, p=0.029$, respectively). t_2 analysis identified late responders profile in 4/5 ill-classified true GHR.

Conclusion: In combination with MR-morphometrics features, DCE-MRI improves response prediction to a-NAC, correlates with % residual viable tumour cells on post-a-NAC surgical specimen, highlights a ‘late-responders’ profile. Estimators of fibrosis and necrosis should be added to the model. Prospective multicentre studies are required for validation.

*

KEYWORDS

Soft-tissue sarcomas; neoadjuvant chemotherapy; DCE-MRI; MRI; treatment response

KEYPOINTS

- DCE-MRI metrics may help to early predict histologic response to a-NAC but further prospective multicentre investigations are required.
- DCE-MRI metrics on pre-operative imaging correlated well with % of viable tumour cells on surgical specimen.
- Inter and intra-observers agreements of relevant DCE-MRI metrics were at least acceptable.
- Multiparametric MRI follow-up enabled to detect ‘late responders’ profile in about 1/3 of good responders.

DISCIPLINE: Thèse de médecine. Diplôme d’étude spécialisé en radiodiagnostic et imagerie médicale

REMERCIEMENTS

Je remercie **l'ensemble des membres du jury** - Pr Thomas Tourdias, Pr Antoine Italiano, Dr François Le Loarer, Dr Eberhardt Stoeckle, Dr Nicolas Alberti, Dr Michèle Kind - d'être ici présents, ainsi que madame le Pr Nathalie Lassau, rapporteur de ce travail. Je porte la plus haute estime à chacun d'entre vous, comme personne et comme médecin. J'espère que ce travail saura être digne de votre attention et éveiller votre curiosité.

Je remercie chaleureusement l'ensemble des médecins de chaque spécialité du **groupe sarcome bordelais** pour leur contribution, à titre de co-auteurs : en anatomopathologie (Dr François Le Loarer, Pr Jean-Michel Coindre), en oncologie médicale (Pr Antoine Italiano, Dr Sophie Cousin, Dr Maud Toulmonde), en chirurgie (Dr Eberhardt Stoeckle, Dr Audrey Michot), en radiothérapie (Pr Guy Kantor, Dr Paul Sargos) et bien entendu en radiologie (Dr Michèle Kind). Je suis honorée de partager les projets de ce groupe, de bénéficier de son ouverture et son dynamisme, et d'espérer pouvoir y contribuer par l'imagerie médicale.

Je remercie **l'équipe de médecine nucléaire** : Dr Anne-Laure Cazeau, Dr Yann Godbert, Dr Axelle Dutertre et Dr Romain Schollammer pour leur soutien, aides, orientations et remarques durant mon dernier stage d'interne en médecine nucléaire.

Je tiens à remercier l'ensemble des manipulateurs en radiologie, en médecine nucléaire, Thomas et Philippe pour l'informatique propre au département d'imagerie, et les techniciens du département d'anatomo-cytopathologie qui nous permettent d'obtenir les données indispensables à ces travaux de recherche en plus de l'activité clinique quotidienne et de ses aléas.

Ces remerciements n'étant pas seulement ceux d'un travail donné, mais aussi ceux d'une période d'étude bientôt révolue, je remercie les personnes, famille, amies/amis proches ou maintenant lointains, qui m'ont fait grandir humainement, culturellement, artistiquement et professionnellement ces six dernières années, ces catégories n'étant heureusement pas exclusives. La liste est longue et j'espère avoir su leur faire ressentir en temps voulu. Peut-être serais-je détrompée, mais, s'il est vrai que découvrir et apprendre reste possible à chaque âge, dans chaque domaine et particulièrement en médecine, la fin de l'internat entrouvre un passage vers un plus grand investissement dans l'apprentissage à autrui et dans l'élargissement des savoirs, passage dont j'espère être à la hauteur.

ABBREVIATIONS

18-FDG-PET/CT: ^{18}F fluorodeoxyglucose positron emission tomography

a-NAC: anthracycline based neo adjuvant chemotherapy

DCE-MRI: diffusion contrast enhanced MRI

DWI: diffusion weighted imaging

FNCLCC: Fédération nationale des centres de lutte contre le cancer

GHR: Good Histological responder

iAUC90: area under the curve at 90s

Ktrans: volume transfert constant

Kep: transfer rate constant

MRI: magnetic resonance imaging

OR: Odds Ratio

PE: Peak enhancement

PHR: poor histological responder

ROC: receiver operator characteristics

ROI: region of interest

SI: signal intensity

STS: soft tissue sarcoma

Ve: extravascular interstitial volume

Vol: volume

Vp: plasmatic volume

WI: weighted imaging

WIn: Wash in

INTRODUCTION

Soft tissue sarcomas (STS) are a heterogeneous group of mesenchymal tumours that can affect any anatomical site, especially extremities and trunk wall.

At a locally stage, the recommended treatment is a wide excision with negative margins (R0) carried out by a surgeon specifically trained in the treatment of STS. Despite optimum local treatment, 35% of patients will develop metastasis and die of their cancer. Two phase III studies have demonstrated potential benefits in overall survival in locally advanced high-grade STS patients treated with anthracycline-based neoadjuvant chemotherapy (NAC), redefining the standard of care of this disease (Issels et al., 2010; Saponara et al., 2017; Pasquali et al., 2017; Gronchi et al., 2017). Despite controversies and lack of validation studies, the efficacy of NAC can be estimated by the histologic response performed on the surgical specimen. It consists in the estimation of % identifiable viable tumour cells, % fibrosis or granulation tissue, % of necrosis on the whole tumour volume (Figure 1.A). Despite controversies and lack of validation studies, by analogy with osteosarcomas, the cut-off to distinguish poor from good histologic responses (PHR and GHR, respectively) is often defined at 10% (Bielack et al., 2002; Previsor et al., 1997, Lucas et al.; 2008; Walderman et al., 2011; Andreou et al. 2015). Recent communication has demonstrated the relevance in multivariate prognosis analysis to predict overall survival (Cousin et al., 2017).

Histologic response can only be performed at the end of NAC. Biopsy under treatment would only estimate the response on a small sample of a heterogeneous lesion, in an unethically invasive manner. Thus, there is a need for STS-specific non-invasive biomarkers in order to monitor the response on the entire tumour volume (Sullivan et al., 2015; FDA-NIH Biomarker working group, 2016).

The most widely used and validated method to assess response is based on variation of tumour maximal length, the basis of the Response Evaluation Criteria in Solid Tumours (RECIST 1.1), whose advantages are reproducibility and ease to measure (Eisenhauer et al., 2009), bi-dimensional (WHO) and volume being classically not used for STS, although their value has not been estimated. Yet, evaluations based on measures do not take into account vascular and architectural alterations that occur before size variation. The poor correlation between RECIST 1.1 and histological and clinical outcomes has been reported, notably in STS (Canter et al., 2010; Le Grange et al., 2014; Messiou et al., 2016) or in the setting of targeted therapies for gastrointestinal stromal tumours, for instance (Benjamin et al., 2007; CHOI et al., 2007). The RECIST working groups continuously investigating adaptation of RECIST, dealing with opposed issues such as innovation, generalization, specificity, feasibility or reproducibility, but none of the recent guidelines include adaptations for STS (Seymour et al., 2017; Litiere et al., 2017; Litiere et al., 2016).

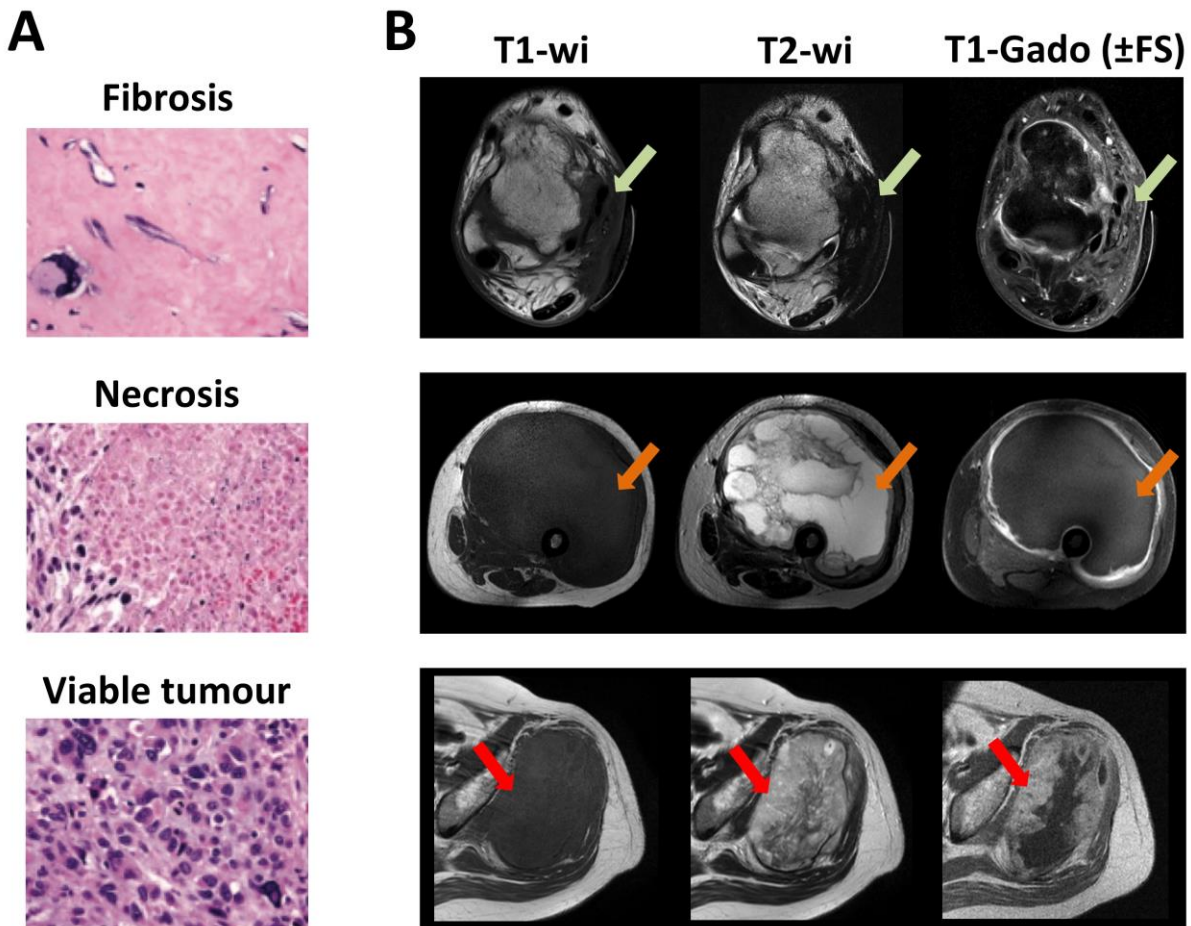


Figure 1. Features of post-NAC post-operative pathological analysis (**A**) and conventional MRI correlates (**B**). **Fibrosis** (green arrow) is characterized by low SI on T1 and T2-wi with late, ill limited, moderately intense enhancement after CA injection. **Necrosis** (orange arrow) is characterized by fluid-like low SI on T1-wi, very high SI on T2-wi, and no enhancement after CA injection. Viable tumour usually show intermediate SI on T1-wi, T2-wi and got enhanced on static post-contrast sequences.

Magnetic resonance imaging (MRI) with contrast agent (CA) intravenous injection can virtually capture fibrosis and necrosis that occurred under NAC (Figure 1.B). However, the early identification of tissues that are getting fibrotic or necrotic remains challenging. These tissues can exhibit continuous alterations from normal tissue to definitive fibrosis or necrosis. In addition, MRI also enables the analysis of tumour margins, surrounding tissue and local bone, nerve and vessels invasions.

Previous studies have already demonstrated improved prediction of prognosis with modified Choi compared with RECIST (Stacchiotti et al., 2009; Stacchiotti et al., 2012). Through a quantification of the enhancing part of the tumour, mChoi aims at estimating the residual viable component and to identify responders without decrease in size. Nonetheless, by being acquired several minutes after Gadolinium chelates injection, mChoi measurements confound enhancement of the residual

viable component resistant to NAC, of the fibrosis, and of components with underlying necrotic or fibrotic processes.

Dynamic-contrast-enhanced MRI (DCE-MRI) is a well-known MR technique that has been notably developed in oncology to non-invasively study blood supply and abnormal vascularization of tumours. Its applications include local staging, NAC response monitoring, and identification of residual or recurrent tumour after surgery (Jackson et al., 2007; Padhani et al., 2010).

According to the Quantitative Imaging Biomarkers Alliance (QIBA) DCE-MRI technical committee, DCE-MRI consists in serial acquisitions of a 3D gradient echo volumetric T1-wi sequence at a short temporal resolution (<10s) prior (for baseline) and after paramagnetic CA IV injection in order to follow its distribution through pathological tumour vessels and through tumour interstitial space.

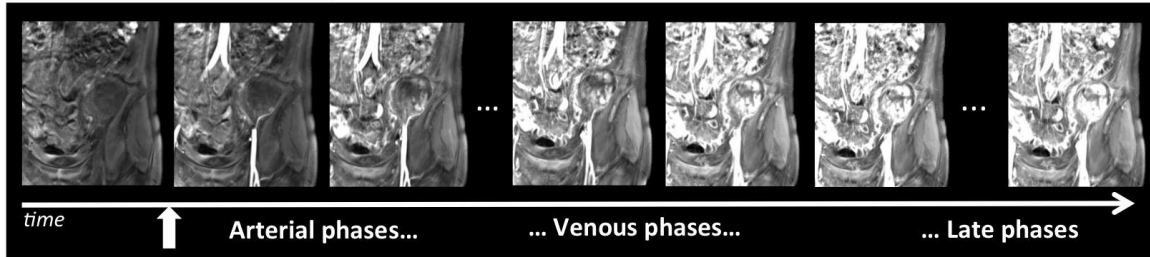
Four levels of DCE-MRI analysis exist (Figure 2):

(i) Qualitative analysis that mainly relies on estimation of enhancement at the first arterial passages and qualification of the enhancement curve of a region or volume of interest (ROI and VOI, respectively) as a function of time,

(ii) Semi-quantitative or model-free analysis, which relies on numeric indices extracted directly from the time-versus-signal intensity (or time-versus-[Gadolinium]) curve (wash-in, wash-out, area under curve, time to peak of enhancement, Peak enhancement, curve wash-out, signal enhancement ratio),

(iii) Quantitative analysis based on permeability multi-compartment pharmacokinetic models. There are pre-requisite before performing this analysis. Indeed, signal intensity variation following CA IV injection is not linearly correlated with CA concentration. To address this issue, it has been proposed to complete a pre-contrast T1 map of the explored volume (Relaxometry or T1 mapping). To correctly convert SI during time, another requirement is classically to calculate a patient-specific arterial input function. The most commonly used and recommended model is the extended Tofts model, a two compartments model (intravascular..

A Raw DCE-MRI data

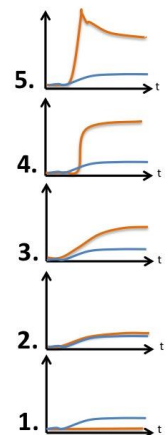
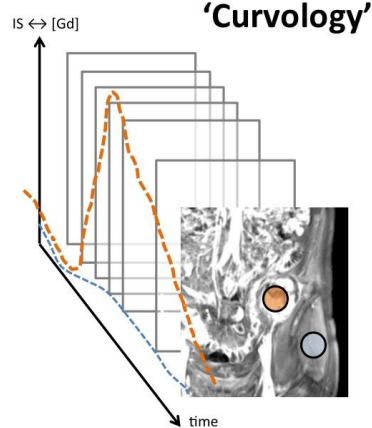
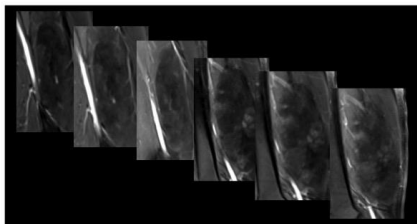


B

Qualitative Analysis

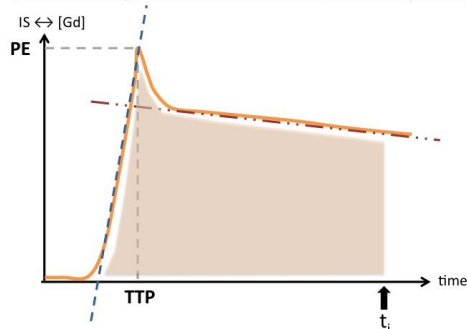
'arterial phase enhancement'

Estimation of % of tumour volume with arterial phase enhancement
($\leq 10\%$ - 10-50 - $> 50\%$)



C

Semi-quantitative Analysis



Model-free quantification of the contrast agent kinetics

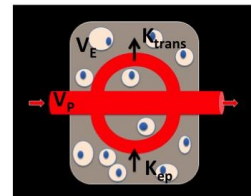
- PE: peak enhancement
- TTP: time to reach the peak
- Wash In (WIn)
- Wash Out (WOut)
- Area under the curve at t_i (AUCi)

D

Quantitative Analysis

Tracer kinetic bi-compartmental Tofts-Kety model

- Relaxometry T1-mapping
- Arterial Input function
- Conversion of T1 signal intensity into paramagnetic CA concentration



$$\frac{dC_{ei}(t)}{dt} = K_{trans} \times C_p(t) - K_{ep} \times C_{ei}(t)$$

- K_{ep} (transfer rate constant, $= K_{trans} / V_{EES}$)
- K_{trans} : volume transfer constant ($\cdot \text{time}^{-1}$)
- V_{Ei} : extravascular, interstitial compartment volume
- V_p : plasmatic volume

Figure 2. Summary of DCE-MRI analyses

..space, IVS, and extravascular extracellular interstitial space, EES) both supposed to be at diffusion equilibrium (Tofts et al., 1999). The model generates two transfer constants: K_{trans} (volume transfer

constant between IVS to EES) and K_{ep} (efflux rate constant, between EES to IVS) and estimates fraction volumes corresponding to EES (v_e) and IVS (v_p).

(iv) The most recent level is texture analysis, which herein would aim at quantifying the vascularization heterogeneity within tumour. The underlying idea of texture analysis is to study all the information that was lost by working on average values of a ROI. Semi-quantitative and quantitative DCE-MRI provide parametric maps for each indices on which can be performed first-order (based on histogram), second order (based on co-occurrence matrices, which can grab the heterogeneity in spatial organization of voxels) or higher order statistics. Among the multiple numeric indices derived from these complex analyses and helped by machine learning approach and classification tasks, some of them, or their combination, could be identified as surrogate biomarkers for prognosis, sensitivity to local (radiotherapy) or systemic (chemotherapy, immunotherapy, targeted therapy) treatments, and histologic response prediction, for instance (Limkin et al., 2017; Gillies et al., 2016; Kumar et al., 2012; Lamblin et al., 2012).

Identification of surrogate biomarkers among DCE-MRI parameters has been extensively studied, especially in solid tumour treated with anti-angiogenic drugs in pre-clinical and prospective trials for prognosis or response under treatment. Conclusions of clinical studies were halftone and did not validate surrogate biomarker, usable in clinical trials or daily practice (Hahn et al., 2008; Morgan et al., 2003; Bahri et al., 2008; Dingemans et al., 2011; Liu et al., 2005).

For mesenchymal tumours, bone sarcomas (osteosarcoma and Ewing sarcoma) were among the first ones to illustrate the potential of DCE-MRI as predictors of histologic response and survival, and to help plan surgery (Hanna et al., 1992; Reddick et al., 1995; Dyke et al., 2003; Egmont-Petersen et al., 2000; Uhl et al., 2006)

DCE-MRI for STS has demonstrated its added value in order to predict malignancy when its qualitative analysis was associated with static post-contrast MRI in a prospective study (Van Rijswijk, 2004), and in order to detect local recurrence (Del Grande, 2014). Nevertheless, this MR method has not been as used as in other solid tumours for treatment response evaluation, because of STS rarity, heterogeneity in term of histotypes, genetics and vascularization.

However, assessment of tumour response to neoadjuvant treatment for STS has demonstrated promising results despite small, retrospective or pre-clinical series with lack of homogeneity in patient population and in definition of tumour response. Actually, some considered a good response depending on % of necrosis other to 0 %, 5%, 50% viable tumour cells (Meyer et al., 2013; Huang et al., 2016; Soldatos et al., 2016, Monsky et al., 2012). Additionally, none of the neoadjuvant treatments (isolated limb perfusion (ILP), chemo-radiation, or non-mentioned) of which the effects

were assessed, represented the currently recommended NAC, that is to say anthracycline-based chemotherapy.

Nonetheless, Soldatos et al. demonstrated in 23 patients the interest of qualitative assessment of arterial phase enhancement with a cut-off of 5% of early-enhanced tumour volume, without mentioning when pre-operative evaluation was performed and which NAC was used (Soldatos et al., 2016). Van Rijswijk depicted the pattern of enhancement as helpful to determine the fibrotic, necrotic or tumour nature of residual lesion after ILP (Van Rijswijk et al., 2003). Recently, Huang et al. demonstrated that K_{trans} was of better value to predict response than %change in longest diameter at 2 weeks. But the studied population was small (N=20), included different neoadjuvant treatments (chemoradiotherapy or sorafenib+chemoradiotherapy) and they did not compare their model of quantitative DCE-MRI with the extended Tofts model recommended by RSNA QIBA alliance (Huang et al., 2016).

In pre-clinical studies with experimental sarcoma mouse model, Alic et al. showed that K_{trans} was significantly reduced in ILP-treated mice, with a decrease of heterogeneity on cumulative histogram of K_{trans} maps, in tumour itself and in tumour periphery (Alic et al., 2013).

Viglianti demonstrated predictive value on overall survival and metastasis free survival of semi-quantitative and quantitative DCE-MRI performed prior and 24h after neoadjuvant hyperthermia/radiation therapy (Viglianti et al., 2009).

To conclude on what has been done until now about DCE-MRI and STS under neoadjuvant treatment, clinical and experimental sets of arguments guide towards potential improvement of response assessment compared with simple measures (such as RECIST1.1). However, several points require to be fixed prior to build prospective studies with decision-making based on DCE-MRI: (i) lack of treatment homogeneity, (ii) lack of definition of optimal moment of evaluation, (iii) lack of validation of most relevant DCE-MRI (iv) lack of association with other MRI modalities, at least morphometrics analysis (v) lack of uniformly accepted definition of histological response, (vi) lack of reproducibility analysis.

Consequently, in an attempt to retrospectively address these issues, the purpose of our study was to perform a large analysis of qualitative, semi-quantitative, quantitative DCE-MRI-derived criteria associated with morphometrics MRI features of tumour itself and tumour periphery, undergoing same recommended a-NAC, at early and similar moment from its beginning, by two independent radiologists. First aim was to determine which conventional MRI and DCE-MRI features on early evaluation could predict histologic response to a-NAC in locally advanced STS patients.

MATERIALS AND METHODS

Our institutional review board approved this retrospective monocentric study and informed consent was waived for each patient.

1. Study population and design (Figure 3)

In total, 46 patients were included in the study between May 2012 and December 2016. They all met the following criteria:

- Newly diagnosed STS of the trunk wall or extremities, with pathological confirmation of the diagnosis in a sarcoma reference centre
- Locally advanced, non-metastatic (assessed at least on chest computed tomography), high grade STS, according to FNCLCC (Guillou et al., 1997)
- Validation of a-NAC during the regional interdisciplinary panel of the sarcoma reference centre with a total of 5-6 cycles.
- Available pre-therapeutic MRI₀
- MRI₁ and DCE-MRI₁ for early evaluation of a-NAC efficacy performed on the same MR-system at 2 to 3 cycles with DCE-MRI and conventional sequences.
- Curative surgery after achievement of the chemotherapy
- Pathologic response assessment on the whole surgical specimen with estimation of % necrosis, % of fibrosis, % of viable tumour cells.

Additionally, all the patients benefited from adjuvant radiotherapy and were followed-up at our institution.

For each patient, the following data were reported: age, gender, ASA score, performance status, tumour location (shoulder girdle, pelvic girdle, upper limb, lower limb, trunk wall), pain at diagnosis, modality of diagnosis (imaging-guided micro-biopsy, surgical biopsy, incomplete surgery performed out of a reference centre and without diagnosis), histotype, delay between MRI₂ and surgery, delay between last cure of a-NAC and surgery.

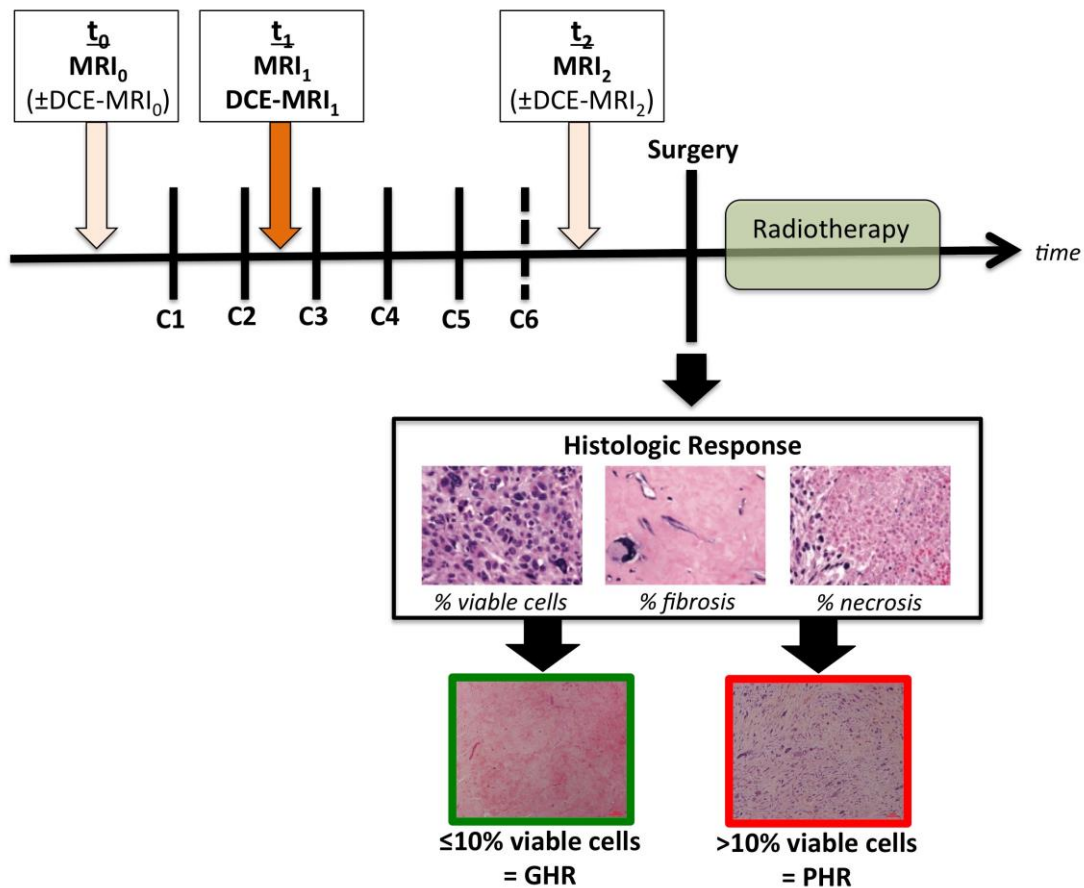


Figure 3. Study design

2. Pathologic examination

Hematoxylin and Eosin-stained slides of the initial diagnostic biopsy and of the surgical specimen were all reviewed by two expert pathologists from our sarcoma reference centre, following published EORTC guidelines (Wardelmann et al., 2016). The percentage of histologically intact viable tumour (% residual viable tumour cells), necrotic tissue (%necrosis) and granulation tissue (%fibrosis) were scored per slide, and the mean weighted percentage for each component was calculated. One can note that %necrosis + % fibrosis + %viable tumour cell = 100%. Patients were classified as GHR if ≤10% of residual tumour cells were seen, and as PHR if >10%, by analogy to the Salzer-Kuntschik grading system for osteosarcoma (Salzer-Kuntschik et al., 1983). Margins status was assessed as being: R0 (macroscopically complete with negative microscopic margins), R1 (macroscopically complete with positive microscopic margins), R2 (macroscopically incomplete), after consensus between surgeon and pathologists.

3. MRI protocol and post-processing

All patients had an initial pre-therapeutic MRI (t_0 : MRI₀), following 2-3 cycles of a-NAC (t_1 : MRI₁), late pre-operative MRI (t_2 : MRI₂)

81.5% (101/124) of the whole set of MRI was performed at our institution (23 initial MRI₀, 46 early MRI₁ and 32 late MRI₂) and 18.5% in external radiological centre (23/124, all being initial MRI₀, conventional without DCE-MRI sequence). These external MRI were included in our picture archiving and communication system (PACS IMPAX v6.5, Agfa, the Netherlands)

At our centre, MR imaging examination were performed on the same 1.5-T MR imaging system (AERA 1.5T Siemens Medical Solutions, Erlangen, Germany) with adapted coils depending on the tumour location. For trunk wall and girdles, a 18-channels phased-array body coil was used. For extremities, a knee 15 channels coil (knee or wrist tumour) or head 32 channels coil (ankle or foot tumour) were used.

3.1. Conventional MRI

At our centre, MRI were acquired during routine clinical practice. At least one T2-wi (turbo spin echo imaging (2D-TSE), repetition time (TR)=3020ms/echo time (TE)=136ms, thickness (th)=4mm), one T1-wi (2D-TSE, TR/TE=557/12ms, th=4mm), one orthogonal fluid-sensitive T2-wi with fat suppression (2D-TSE, TR/TE=4150/69ms, th=4mm) and one T1-wi after fat suppression and gadolinium chelates injection (3D-Dixon EDG TR/TE=6.8/2.3ms, flip angle= 10°, isotropic resolution 1mm, with multiplanar reformation), following DCE-MRI had to be available. MRI performed in other centre had to include at least two orthogonal plans in order to measure the maximal length for RECIST 1.1, the two diameters for bi-dimensional and the volume assessments.

3.2. DCE MRI sequences acquisition and post-processing

Acquisition. Before the DCE-MRI acquisition, data for constructing a T1 map were acquired with a spoiled 3D gradient echo T1-wi sequences (TR/TE=1.82/4.65, th=1mm, intersection gap: 10-20% (depending tumour size), FOV=240mm, matrix= with 2° and 15° flip angles)

The same volume acquisition was used for DCE-MRI sequence, which consisted in a 3D fast spoiled gradient echo sequence with following acquisition parameters: TR/TE = 4.3/1.7ms, flip angle =20°, FoV and Matrix adjusted for in plane resolution of 1,1x1,1mm, th=4mm. The volume acquisition was repeated every 8-9 seconds. At least two baseline volume acquisitions were performed prior to contrast agent injection, followed by 18 volumes after. The whole DCE-MRI lasted about 3mn30s.

0.1mM/kg of Gadoteric acid (Guerbet, France) or Gadobenate Dimeglumine (Bracco, Italy) were injected intravenously at a rate of 2mL/sec followed by a 20 mL flush of 0.9% f NaCl solution helped by a MR compatible automatic injector (Sonic Shot 7, Nemoto Kyorindo, Japan)

Post-processing. DCE-MRI were post-processed with dedicated OleaSphere software (Olea Medical, version 3, La Ciotat, France) by the same radiologist (Rad1). T1-mapping was performed with Relaxometry module to generate R0- R1- T1- T0- maps that were used to optimize DCE-MRI

consecutive analysis. Depending on the contrast agent injection, signal intensity was converted in Gadolinium concentration ([Gd]).

Motion artefacts were corrected with a rigid-body coregistration method. The arterial input function was semi-automatically determined helped by cluster analysis technique with manual adjustment if required after control quality (Mouridsen et al., 2006). Permeability module was used to generate semi-quantitative (Wash-In, Peak-Enhancement, AUC at 90 s) and quantitative (K_{trans}) parametric maps.

Wash-In (WIn, $\text{mmol.L}^{-1}.\text{s}^{-1}$) corresponds to the velocity (or mean slope) of the increasing part of the curve, that is to say to the initial and mean gradient of the upsweep of the enhancement curve, calculated with linear least square method.

Peak-enhancement (PE, %) corresponds to the % of increase of the initial up-slope of the curve during the acquisition time.

iAUC90 is the area under the time-vs-[Gadolinium] curve following the 90s after detection of contrast agent detection. It represents a mix between blood volume and permeability.

We decided not to generate parameters related to return transfer of contrast agent from EES to IVS (Wash-out, K_{ep}) because our acquisition was limited to 3mn30 in order to focus on the early phases of the enhancement and because our protocol was integrated in the daily practice with time constraint and risk of motion artefact.

Control quality. Global quality of the arterial input function and parametric maps were estimated according to a 3 points-scale (0: non-diagnosis DCE-MRI, 1: poor quality non-usable for quantification, 2: good). Miscalculations on K_{trans} map, defined as discordance between tumour enhancement on raw data and K_{trans} map, were reported and excluded for quantitative analysis.

4. Reader procedure

Two radiologists (Ra1 and Ra2, with 2 and 25 years of experience in musculoskeletal soft-tissue tumours MRI, respectively), blinded to the imaging and histopathology reports, independently evaluated the MRI studies. Ra1 performed two lectures with a delay of 2 months between the 2 sessions. The order of MRI reading was randomly modified for the second session to limit memory bias. For imaging criteria based on qualitative assessment of conventional MRI, a final consensual reading between Ra1 and Ra2 was made in case of interpretation disagreement.

4.1. Conventional MRI analysis

Location. Tumour was qualified as deep, deep + superficial and superficial, depending on its situation relative to the superficial aponeurosis.

Measurements. For each MRI (t_0 , t_1 , t_2), radiologists determined the maximal length of the tumour (L1), the two diameters ('a x b') on the maximal surface on axial sequence. Additionally, Ra1

manually segmented all the tumours on T2-wi sequence, slice-by-slice, with the help of other sequences for more accurate delineation, in order to calculate tumour volume (Vol).

Tumour Architecture. Each radiologist estimated the percentage of necrosis, fibrosis and haemorrhage on a three points scale (0: $\leq 10\%$, 1: 10-50%, 2: $\geq 50\%$). Necrosis was defined as component with very low signal intensity (SI) on T1-wi, fluid-like very high SI on T2-wi, with irregular borders and without enhancement after CA injection. Fibrosis was defined as component with very low SI on T1-wi and T2-wi, below muscle SI, with possible late enhancement. Haemorrhage was defined as a component with high SI on T1-wi, remaining high on T1-wi with fat suppression.

Tumour Periphery and local extension. Radiologists reported the presence or absence (1 or 0) of (1) ill-defined margins (2) peripheral oedema on T2-wi with fat suppression, (3) enhancement of the oedema after CA injection and (4) vascular, nervous and/or bony invasion.

T2-ratio. Relative T2-ratio ($= SI_{\text{tumour}}/SI_{\text{muscle}}$) is a numeric parameter that was introduced to assess response in rectal cancer with decrease of this ratio being interpreted as a reflection of fibrosis (Kluza et al., 2013). $T2\text{-ratio} = SI_{\text{tumour}}/SI_{\text{muscle}}$ where a region of interest (ROI) is drawn on a representative surface of the tumour to obtain SI_{tumour} , and a second ROI is carefully drawn on a healthy muscle of other muscular lodge, avoiding intramuscular fat to obtain SI_{muscle} .

Variations under treatment (0 \rightarrow 1, 0 \rightarrow 2). $RECIST_{0 \rightarrow 1}$, $RECIST_{0 \rightarrow 2}$, $WHO_{0 \rightarrow 1}$, $WHO_{0 \rightarrow 2}$, $\Delta Vol_{0 \rightarrow 1}$, $\Delta Vol_{0 \rightarrow 2}$ were calculated for each patient. Apparition of sero-hematic levels within the tumour was reported. Variations of tumour architecture and tumour periphery variables were qualified as 0: similar, 1: decreased, 2: increased.

Different types of changes could be assessed: mainly fibrotic, mainly necrotic, mixed fibro-necrotic and no evolution. Among those with fibrotic changes, we distinguished a pattern consisting in large fibrosis of the tumour, while a nodular tissue component was absolutely unaffected on conventional sequence (Figure 4) with a tendency to grow, suggesting resistance to a-NAC. We called this 'compartmental fibrosis' (to differentiate it from peripheral fibrosis, diffuse internal fibrosis, internal septa fibrosis, no fibrosis).

Finally, on T1-wi and T2-wi, radiologists were asked to estimate on a 3 point-scale the variation of heterogeneity (0: less heterogeneous, 1: similar, 2: more heterogeneous)

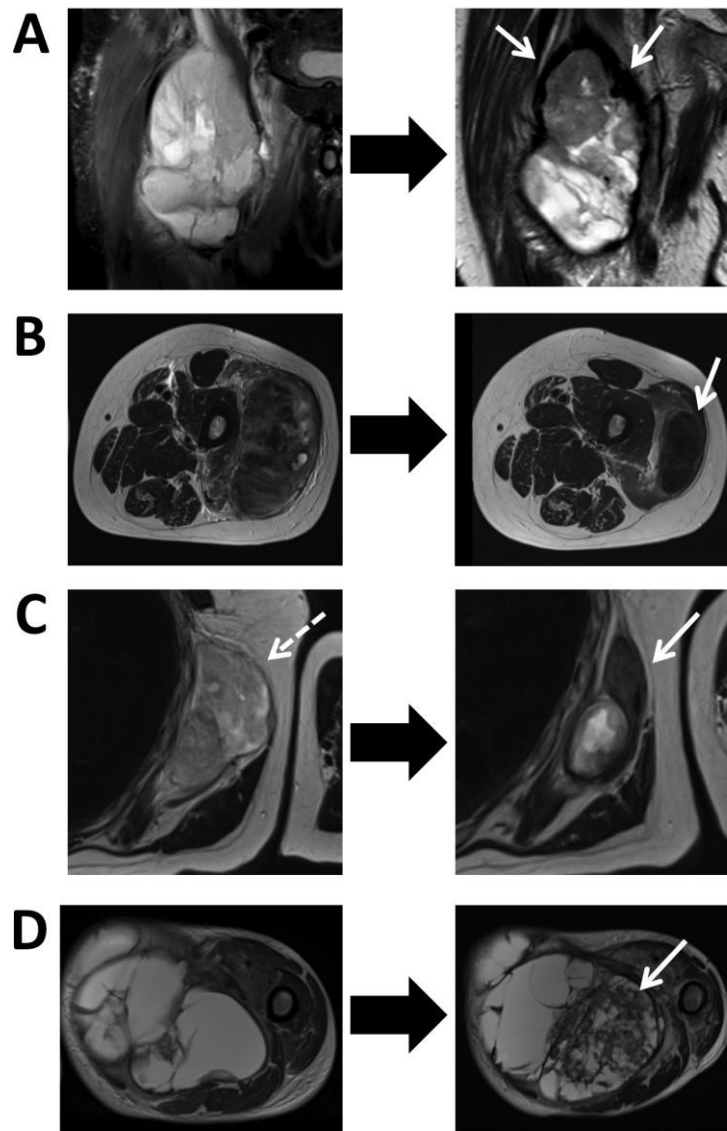


Figure 4. Pattern of fibrosis on conventional T2-wi. (A) **Peripheral fibrosis** : apparition of a thick coating with low SI on T2-wi (white arrow). (B) **Diffuse entire fibrosis** of a grade III leiomyosarcoma (confirmed on pathological analysis where %fibrosis = 95%) (C) **Compartmental fibrosis** in a poor responders. The anterior component of this grade III UPS showed a decrease of SI on T2-wi compatible with fibrosis (white arrow), while it initially demonstrated similar SI (dotted line) to the posterior, apparently-resistant- nodule. (D) **Septa fibrosis** : a mesh of severable septa of low T2-SI appeared within a necrotic compartment of a grade III myxofibrosarcoma.

4.2.DCE-MRI analysis (Figure 5)

ROI positioning. The two radiologists had to manually place three ROI that were propagated on the set of parametric maps (W_{in} , PE, $iAUC_{90}$, K_{trans}). Conventional MRI and DCE-MRI were all available to help ROI placement. One ROI was placed on the maximal surface of the whole tumour (ROI_S), one ROI of at least $1cm^2$ was placed on the first component of the tumour that displayed CA uptake on raw DCE-MRI data (ROI_N , supposed to represent its most aggressive component) and one ROI on healthy muscle from another muscular lodge (reference ROI_M)

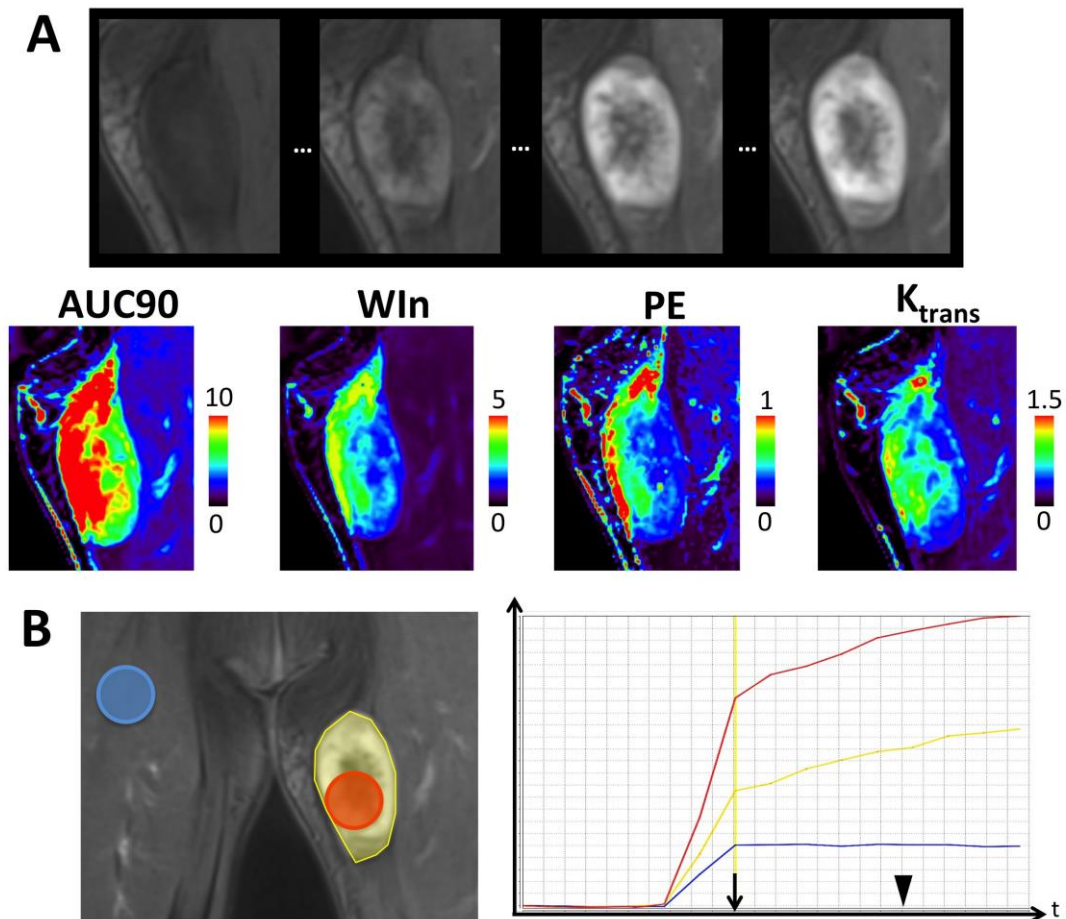


Figure 5. DCE-MRI data sets available in order to place the regions of interest (ROI) (A), including raw DCE-MRI (upper images) to identify which was the first area of the tumour to firstly show CA uptake. (B) Three ROI were manually drawn: one circular of at least 1cm² on this area (ROI_N, red), one on the maximal surface of the tumour (ROI_S, yellow), and one on healthy muscle from another lodge. (C) shows the curves for each ROI with corresponding colours (black arrow: time to the peak enhancement, arrow head: t=90s for AUC90)

Qualitative analysis. On raw DCE-MRI data, radiologists identified the sequences that were acquired prior to venous filling, on which they estimated the percentage of arterial enhancement of the tumour (0: ≤10%, 1: >10%).

After ROI placement, they qualified the morphology of the time-vs-[Gd] curve for ROI_S and ROI_N according to a two points-scale (1: slope and/or plateau ≥ 3 x slope and/or plateau of the healthy muscle ROI₃, 0: below). In case of disagreement between the readers during the consensual reading, the most unfavourable option (1) was taken.

Semi-quantitative and quantitative analyses. Indices value for each ROI was reported in order to calculate the following parameters:

Absolute value: X-ROI_{i,j}

Ratio relative to the healthy muscle: X-ratio-ROI_{i,j} = X-ROI_{i,j} / X-ROI_{M,j}

Where $i \in \{s,n\}$, corresponding to the two tumour ROIs, $j \in \{0,1,2\}$, corresponding to the time of evaluation, and $X \in \{Ktrans, WIn, PE, iAUC90\}$. Thus, a total of $4 \times 4 = 16$ parameters were available for each MRI, as well as their change, exposed as:

$$\%Change-X_{0 \rightarrow j} = 100 \times (X-ROI_{i,j} - X-ROI_{i,0}) / X-ROI_{i,0}$$

$$\%Change-X-ratio_{0 \rightarrow j} = 100 \times (X-ratio-ROI_{i,j} - X-ratio-ROI_{i,0}) / X-ratio-ROI_{i,0}$$

5. Statistical analysis

-Normality was assessed for each continuous value by using Shapiro-Wilk test. Depending on the results, the student t-test or the Mann-Whitney U-test was performed to compare good and poor histologic responders.

-Categorical and ordinal parameters were compared using the Chi-2 or Fisher test

-For significant association between continuous parameters and histologic response, receiver-operating curves were built in order to quantify the performance of each individual parameter and to find the optimal cut-off points that satisfy the Youden index (i.e. point farthest from chance, to minimize rate of misclassification) (Perkins, 2006). Sensibility (Se), specificity (Sp), odd-ratios (OR) with 95% confidence interval (CI_{95%}) for these cut-off points were calculated. Thus these continuous variables were dichotomised (0: under the cut-off, 1: above).

- The relevant clinical variables, conventional MRI₁ variables, DCE-MRI₁ variables, all dichotomised as dummy variable, were analysed in multivariate analysis by using a binary logistic regression, with entry method, to estimate multivariate OR with their IC. Collinearity diagnostic was previously tested. The adequation of the multivariate model was assessed with Hosmer-Lemeshow test and with R²-nagelkerke index. The ROC curve of the multivariate model at t1 was built and compared with ROC curves of % change of maximal size (RECIST 1.1) and each individual relevant DCE-MRI₁ parameters.

-Correlation between the imaging parameters that were significantly associated with histologic response on late MRI₂, and the percentage of viable tumour cells, were estimated using univariate linear regression (with Spearman's rank correlation or Pearson test depending on normality test result), followed by multivariate linear regression.

-The inter- and intra-observers reliabilities were assessed using interclass correlation coefficient (ICC) for continuous values (with two-way mixed and one-way random models respectively). The Cohen's Kappa (κ) test for pairwise agreement was used for dichotomous variable. Weighted kappa (κ_w) statistics was used for ordinal variable (herein RECIST 1.1 and OMS at early (0→1) and late (0→2) evaluations).

The agreement for ICC was defined as good (>0.75), moderate (0.5-0.75) or poor (<0.5). The agreement for classical κ and κ_w was defined as slight (0-0.20), fair (0.21-0.40), moderate (0.41-0.60), substantial (0.61-0.80) and almost perfect (0.81-0.99) (Landis, 1977).

-All tests were two-tailed. Statistical analyses were done using GraphPad Prism (GraphPad Software, Inc., version 7, La Jolla, CA) and the SPSS statistical package (IBM, version 21.0, Chicago, IL) with Python plug-in. A p-value of less than 0.05 was deemed significant.

*

RESULTS

1. Clinical patient data (Table 1)

From May 2012 to December 2016, 46 patients (18 female) met inclusion criteria and completed conventional MRI₀ and DCE-MRI₁, 23/46 (50%) also having DCE-MRI₀ and 32/46 (69.6%) DCE-MRI₂. Thus, among them, 23/46 (50%) had both DCE-MRI₀ and DCE-MRI₁ and 17/46 (37.0%) had DCE-MRI₀ and DCE-MRI₂.

Median age was 58 years (range, 33 - 77)

Median time between baseline MRI₀ and the first cycle of treatment administration was 28 days (range, 0 - 94).

Median time between last cycle of a-NAC and surgery was 29 days (range, 19 - 81).

Median time between MRI₂ and surgery was 25 days (range, 1- 50).

34/46 (73.9%) were classified as PHR and 12/46 (26.1%) as GHR after pathological analysis on surgical specimen.

Table 2 summarizes the salient initial clinical and histological features.

Among the 18 included females, only 1/18 (5.5%) was GHR, while 17/28 (60.7%) males were GHR ($p=0.015$, $OR_{univariate} = 11$ (1.42 – 124.60))

Table 1 : Clinical Features of the study population

	<u>GHR (n = 12)</u>	<u>PHR (n = 34)</u>	Total
Age (years)	55.5 (39-71)	58 (33-77)	58 (33-77)
Gender - F - M	1/12 (%) 11/12 (%)	17/34 (50%) 17/34 (50%)	18/46 (39.1%) 28/46 (60.9%)
ASA score - 1 - >1	4/12 (33.3%) 8/12 (66.6%)	12/34 (35.3%) 22/34 (64.7%)	16/46 (34.8%) 30/46 (65.2%)
Initial pain - yes - no	7/12 (58.3%) 5/12 (41.7%)	21/33 (61.8%) 12/33 (35.3%)	28/45 (62.2%) 17/45 (37.8%)
Site group - Shoulder girdle - Upper limb - Trunk wall - Pelvic girdle - Lower limb	2/12 (16.7%) 2/12 (16.7%) 2/12 (16.7%) 1/12 (8.3%) 5/12 (41.7%)	3/34 (8.8%) 4/34 (11.8%) 2/34 (5.9%) 1/34 (2.90%) 24/34 (70.6%)	5/46 (10.9%) 6/46 (13%) 4/46 (8.7%) 2/46 (4.3%) 29/46 (26.1%)
Depth - Superficial - Superficial and deep - Deep	0/12 (0%) 4/12 (33.3%) 8/12 (66.6%)	2/34 (5.9%) 8/34 (23.5%) 24/34 (70.6%)	2/46 (4.3%) 12/46 (26.1%) 32/46 (69.6%)
Histotypes - Undifferentiated sarcomas ¹ - Muscular sarcomas ² - M-RC LPS ³ - Other LPS - Synovialosarcoma - MPNST	6/12 (50%) 3/12 (25%) 0/12 (0%) 2/12 (16.7%) 1/12 (8.3%) 0/12 (0%)	15/34 (44.1%) 8/34 (23.5%) 6/34 (17.6%) 1/34 (2.9%) 3/34 (8.8%) 1/34 (2.9%)	21/46 (45.7%) 11/46 (23.9%) 6/46 (13%) 3/46 (6.5%) 4/46 (8.7%) 1/46 (2.2%)
Delay last cycle of a-NAC to surgery (days)	29.5 (21-39)	29 (19-81)	29 (19 - 81)

¹ undifferentiated epitheloid/spindle cell/pleomorphic sarcoma, undifferentiated sarcoma not otherwise specified ;

² rhabdomyosarcoma, leimyosarcoma ;

³ dedifferentiated LPS, pleomorphic LPS

LPS : liposarcoma, M-RC LPS : myxoid-round cell LPS ; MPNST : malignant peripheral nerve sheath tumour

2. Measurements, RECIST1.1, OMS and volume (Table 2, Figure 6)

Initial metrics. There was no significant difference between GHR and PHR at baseline for maximal length, ‘a x b’ and Volume.

$t_0 \rightarrow t_1$. Percentages of maximal length, ‘a x b’ and volume change (%Change- $L1_{0 \rightarrow 1}$, %Change- $axb_{0 \rightarrow 1}$, %Change- $Vol_{0 \rightarrow 1}$) did not exhibit significant difference either from MRI₀ to MRI₁.

Thus, according to RECIST1.1, 3/34 (8.8%) PHR were ill-classified as partial response, 3/34 (8.8%) PHR were well-classified as progressive disease, and 28/34 (82.4%) were classified as stable disease. According to OMS, 4/34 (11.8%) PHR were ill-classified as partial response, 6/34 (17.6%) were well classified as progressive disease, 24/34 (70.6%) PHR were classified as stable disease.

$t_0 \rightarrow t_2$. At final MRI₂ evaluation, %Change- $L1_{0 \rightarrow 2}$, %Change- $axb_{0 \rightarrow 2}$ and %Change- $Vol_{0 \rightarrow 2}$ were all significantly decrease in GHR compared with PHR (p=0.012, p=0.010, p=0.031, respectively)

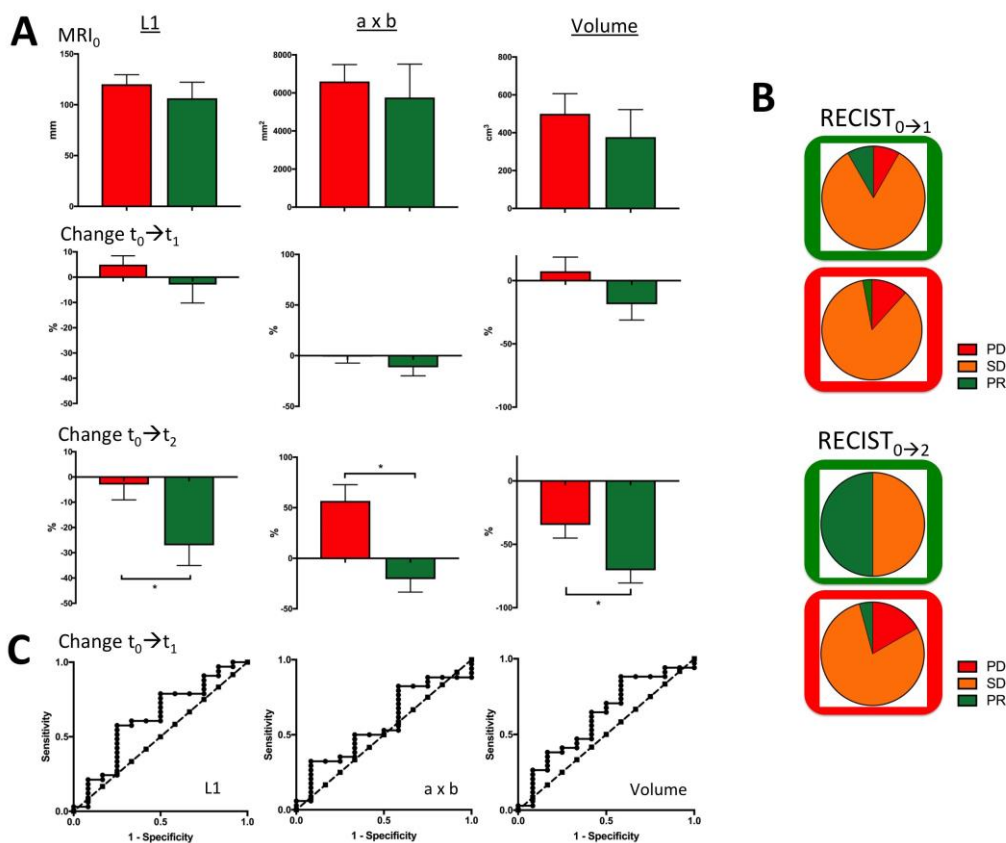


Figure 6. Measurements. (A) longest diameter L1, bi-dimensional diameter ‘axb’ and volume) at t_0 , t_1 , t_2 and change from t_0 to t_1 and t_0 to t_2 . * p<0.05. (B) RECIST1.1 classification at early and late evaluation (PR=partial response, SD=stable disease, PR=progressive disease). Green and red frames correspond to true GHR and true PHR respectively. (C) Area under the ROC curves for %change of longest diameter, bi-dimensional diameter and volume at early evaluation (t_0 to t_1) (not significant p>0.05)

Table 2 : Measurements

	<u>Maximal Length (mm)</u>			<u>a x b (cm²)</u>			<u>Volume (cm³)</u>		
	PHR	GHR	p-value	PHR	GHR	p-value	PHR	GHR	p-value
t₀	120 ± 9,4	106 ± 15,8	0,407 (mw)	66,0 ± 8,9	57,6 ± 17,6	0,451 (mw)	499 ± 107	376 ± 146	0,328 (mw)
%Change t₀ → t₁	4,9 ± 3,5	-2,9 ± 7,3	0,278 (t)	-0,2 ± 7,1	-11,5 ± 8,4	0,466 (mw)	7,3 ± 11,2	-18,7 ± 12,4	0,228 (mw)
%Change t₀ → t₂	-3,0 ± 6,1	-27,7 ± 8	0,012 * (mw)	72,7 ± 22,2	-20,6 ± 12,9	0,010 * (mw)	-4,1 ± 32,5	-70,4 ± 28,4	0,031 * (mw)

* p<0,05

t : Student t-test, mw : Mann-Whitney test

3. Conventional MRI data (Table 3)

Initial features. No significant difference was found between GHR and PHR at baseline, whatever the location, the architectural features, and the peripheral features.

$t_0 \rightarrow t_1$. From MRI₀ to MRI₁, there was a tendency towards a decrease of the initial peripheral oedema, without reaching significance (p=0.054).

Distribution of %fibrosis was significantly different between PHR and GHR (p=0.008) with 1/34 (2.9%) PHR who had qualitatively more than 50% of its volume exhibiting a MRI signal compatible with fibrosis versus 4/12 GHR (33.3%). 11/34 PHR (32.4%) showed a compartmental fibrosis pattern, versus only 1/12 (8.3%) GHR. Despite no significance, this observation suggests that occurrence of a growing tissue nodule within a tumour tending to get fibrotic should suggest a poor response.

$t_0 \rightarrow t_2$. From MRI₀ to MRI₂, there was a significant difference between PHR and GHR for the fibrotic pattern (p=0.041).

T2-ratio, T2-SD-ratio at t_0 , t_1 and t_2 , and their %change from t_0 to t_1 and t_0 to t_2 did not show significant difference.

4. DCE-MRI data

A total of 101 DCE-MRI were acquired (23 DCE-MRI₀, 46 DCE-MRI₁ and 32 DCE-MRI₂). 7 were considered as non-diagnostic for any type of DCE-MRI analysis. Among the 94 remaining DCE-MRI, 12 displayed mismatches between raw data and K_{trans} map, that is to say, highly and early perfused tumour with K_{trans} values equal 0. Thus, a total of 82 DCE-MRIs were used for K_{trans} -related analyses.

Qualitative analysis. Analysis of the curve morphology on ROI_s or ROI_n did not reveal significant difference between GHR and PHR at t_1 . However, at t_2 , 15/24 (62.5%) PHR showed a type 3+4 curves for the ROI_n on versus none of the GHR (0/8, 0%) (p=0.003).

Estimation of less than 10% of tumour volume with arterial phase enhancement did not differ between GHR and PHR at t_1 : 4/34 (11.8%) PHR and 3/12 (25%) GHR displayed this feature. At t_2 , this became significantly different: (3/24 (12.5%) PHR versus 6/8 (75%) GHR, p=0.002).

Semi-quantitative and quantitative analyses. Table 4 and Figure 7 summarize the results for each parameter for each time point. Overall, at t_1 , WIn-ratio-ROI_n was significantly lower for GHR than for PHR (4.78 ± 1.19 versus 9.8 ± 1.65 , p=0.048), as well as PE-ROI_n (93.43 ± 25.62 versus 166.9 ± 96.72 , p=0.029). At t_2 , WIn-ratio-ROI_n and PE-ROI_n were still significantly lower for GHR (p=0.022 and p=0.023, respectively), as well as iAUC90-ratio-ROI_n (p=0.020)

Table 3 : Conventional MRI features at first evaluation t1

	<u>PHR</u>	<u>GHR</u>	p-value
%Necrosis - ≤10% - 10-50% - ≥50%	18/34 9/34 7/34	5/12 3/12 4/12	0.659
%Fibrosis - ≤10% - 10-50% - ≥50%	17/34 16/34 1/34	6/12 2/12 4/12	0.008 **
%Haemorrhage - ≤10% - 10-50% - ≥50%	24/29 3/29 2/29	7/9 1/9 1/9	0.914
Variation of %Necrosis - Decreased + similar - Increased	1+21/33 11/33	1+3/12 8/12	0.086
Variation of %Fibrosis - Similar - Increased	11/33 22/33	4/12 8/12	>0.999
Variation of %Haemorrhage - Decreased - Similar - Increased	4/30 19/30 7/30	2/11 6/11 3/11	0.868
Sero-hematic levels - Yes - No	4/34 30/34	1/12 11/12	>0.999
T1-Heterogeneity variation - Decreased - Similar - Increased	1/22 12/22 9/22	1/8 4/8 2/8	0.622
T2-Heterogeneity variation - Decreased - Similar - Increased	3/32 7/32 22/32	0/11 4/11 7/11	0.420
Margin variation - Still well-limited - Similar or worst delimitation - Better delineation	12/34 20/34 2/34	5/12 5/12 2/12	0.414
Oedema variation - Still no edema - Similar or increased - Decreased	5/18 11/18 2/18	2/8 4/8 2/8	0.661
Peripheral enhancement variation - Still no enhancement - Similar or increased - decreased	9/34 20/34 5/34	3/12 7/12 2/12	0.985
Fibrotic pattern - Compartmental fibrosis - Other (no fibrosis, septa, peripheral fibrosis, diffuse fibrosis)	11/34 23/34	1/12 11/12	0.141

	Wash-In				Peak Enhancement				iAUC90				K _{trans}				
	ROI _k	Ratio-ROI _k	ROI _k	Ratio-ROI _k	ROI _k	Ratio-ROI _k	ROI _k	Ratio-ROI _k	ROI _k	Ratio-ROI _k	ROI _k	Ratio-ROI _k	ROI _k	Ratio-ROI _k	ROI _k	Ratio-ROI _k	
t ₀	PHR	5.0±0.8	12.6±2.9	6.0±0.8	159.3±23.1	96.0±20.4	24.8±8.9	16.9±7.6	15.9±2.1	8.8±1.5	13.0±2.0	7.4±1.7	0.82±0.14	13.6±2.9	0.34±0.05	13.6±2.9	5.8±1.4
	GHR	3.2±1.2	10.9±3.3	4.3±1.4	49.9±25.2	21.4±6.9	12.9±3.3	5.0±1.4	15.7±6.5	5.1±1.4	10.6±2.7	4.2±1.2	0.98±0.55	19.9±10.9	0.41±0.26	19.9±10.9	5.5±3.3
	p.n	0.153 (13; 4)	0.968 (13; 4)	0.968 (13; 4)	0.037* (17; 4)	0.052 (17; 4)	0.698 (17; 4)	0.897 (17; 4)	0.360 (16; 5)	0.360 (16; 5)	0.218 (16; 5)	0.719 (16; 5)	0.319 (16; 5)	0.672 (13; 4)	0.672 (13; 4)	0.785 (13; 4)	0.806 (13; 4)
t ₁	PHR	4.4±0.6	9.8±1.6	5.2±0.8	166.9±16.6	84.7±10.7	15.9±3.4	7.6±1.7	16.3±1.9	9.2±1.4	12.1±1.9	10.0±3.8	1.28±0.31	12.5±3.0	0.50±0.13	12.5±3.0	5.2±1.4
	GHR	3.0±1.0	4.8±1.2	4.7±1.4	93.4±25.6	55.7±20.7	6.6±1.0	3.8±0.6	32.1±18.6	7.0±1.3	12.4±5.1	4.1±1.5	1.13±0.60	10.3±4.8	0.64±0.33	10.3±4.8	5.5±3.3
	p.n	0.144 (34; 11)	0.144 (34; 11)	0.506 (34; 11)	0.029 (34; 11)	0.199 (34; 11)	0.052 (34; 11)	0.115 (34; 11)	>0.999 (34; 11)	>0.999 (34; 11)	0.584 (34; 11)	0.382 (34; 11)	0.137 (34; 11)	0.535 (27; 9)	0.382 (27; 9)	0.450 (27; 9)	0.932 (27; 9)
t ₂	PHR	2.8±0.5	7.9±1.4	5.0±1.1	124±20.1	57.5±11.4	31.5±14.6	21.0±11.1	12.9±2.3	6.9±1.6	11.1±2.9	6.6±2.1	0.74±0.16	7.7±1.2	0.33±0.07	7.7±1.2	3.7±0.6
	GHR	1.7±1.0	4.0±2.1	3.6±5.8	45.3±18.4	36.1±14.4	5.2±1.8	3.9±0.8	6.2±2.1	4.8±1.5	4.8±1.8	3.8±4.5	0.23±0.14	2.2±1.0	0.14±0.06	2.2±1.0	1.6±0.6
	p.n	0.063 (24; 8)	0.241 (24; 8)	0.115 (24; 8)	0.023* (24; 8)	0.255 (24; 8)	0.057 (24; 8)	0.983 (24; 8)	0.060 (24; 8)	0.060 (24; 8)	0.454 (24; 8)	0.020* (24; 8)	0.379 (24; 8)	0.009** (19; 8)	0.043* (19; 8)	0.009** (19; 8)	0.021* (19; 8)
%Change t ₀ → t ₁	PHR	61.4±43.5	56.2±40.8	71.4±41.1	113.5±47.8	94.4±37.8	38.1±21.0	39.5±27.6	30.7±19.8	73.9±45.2	73.9±45.2	13.3±19.3	84.0±80.7	67.5±81.9	85.8±68.8	67.5±81.9	61.5±66.4
	GHR	8.0±2.0	-33.7±12.5	-42.4±39.4	-45.4±30.3	-50.3±30.8	-51.4±13.3	-6.8±43.7	-6.8±43.7	-8.5±46.4	-37±16.3	-37±16.3	-63.7±15.7	-77.8±6.3	-73.3±4.4	-73.3±4.4	-78.8±23.1
	p.n	0.248 (16; 4)	0.117 (16; 4)	0.064 (16; 4)	0.040* (17; 3)	0.028* (17; 3)	0.054 (17; 3)	0.765 (17; 3)	0.765 (17; 3)	0.262 (15; 4)	0.885 (15; 4)	0.152 (15; 4)	0.88 (11; 3)	0.88 (11; 3)	0.060 (11; 3)	0.060 (11; 3)	0.060 (11; 3)
%Change t ₀ → t ₂	PHR	-30.4±19.8	-22.3±21.4	14.3±36.6	30.6±29.2	44.5±30.5	-5.2±26.1	-16.2±62.8	-11.0±18.5	12.1±23.9	-5.7±85.8	9.8±25.4	-21.9±19.7	-24.8±36.6	-22.1±15.0	-24.8±36.6	-32.3±25.6
	GHR	-67.5±24.5	-17.8±61.4	-12.3±46.7	-77.8±11.8	-40.8±26.2	-80.6±9.7	-34.7±35.2	-34.7±35.2	-70.4±42.2	-42.7±37.6	-60.9±29.2	-87.9±5.2	-19.2±10.9	-62.1±21.6	-87.9±5.2	-76.4±12.2
	p.n	0.102 (13; 4)	0.477 (13; 4)	0.703 (13; 4)	0.014* (13; 3)	0.294 (13; 3)	0.057 (13; 3)	0.900 (13; 3)	0.900 (13; 3)	0.078 (12; 4)	0.245 (12; 4)	0.262 (12; 4)	0.703 (12; 4)	0.050 (9; 4)	0.106 (9; 4)	0.050 (9; 4)	0.106 (9; 4)

Table 4: DCE-MRI semi-quantitative and quantitative parameters: values and comparisons between PHR and GHR at t₀, t₁, t₂ and % of change from t₀ to t₁ and to t₂.

(Each case is filled as follows: first line: values ± SEM for PHR, second line: values ± SEM for GHR, third line: p-value and effectives for (PHR; GHR))

and K_{trans} -ROI_s, K_{trans} -ROI_n, K_{trans} -ratio-ROI_s, K_{trans} -ratio-ROI_n (p=0.043, p=0.009, p=0.021 and p=0.009, respectively)

Determination of optimal threshold for significant criteria at t₁. For WIn-ratio-ROI_n, ROC analysis demonstrated an AUC=0.70 (0.53-0.87). Optimal threshold, was 3.48 mmol.L⁻¹.s⁻¹ (Youden index = 0.03) leading to Se=0.79, Sp=0.55, PPV=0.84, OR_{univariate}=5.40 (1.17, 23.72) to detect PHR.

For PE-ROI_n, AUC was 0.71 (0.54-0.89). Optimal threshold was 143.5%. (Youden index = 0.49) providing Se=0.68, Sp=0.83, PPV=0.92, OR_{univariate}=10.45 (1.99-51.22) to detect PHR.

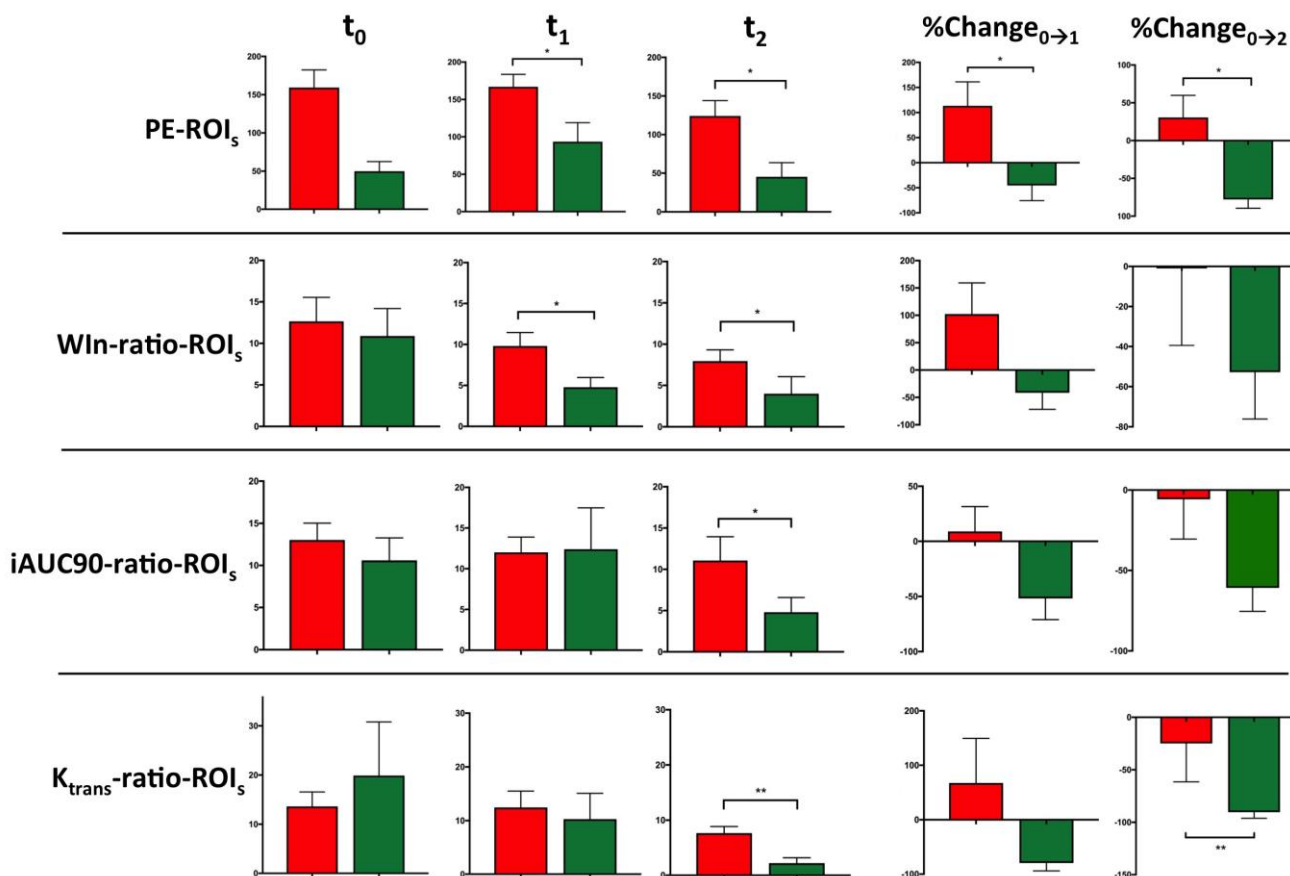


Figure 7. Values (at t₀ t₁ and t₂) Variation (from t₀ to t₁ and 1 to t₂) of DCE-MRI semi-quantitative and quantitative indices. * p<0.050, ** p<0.010.

5. Inter and intra observer agreements of the relevant criteria at t₁ and t₂

Table 5 shows the agreements for each relevant criterion among measures, conventional MRI and DCE-MRI studies. None of the conventional MRI criteria showed both inter- and intra-reader at least substantial agreement. At t₁ and t₂, PE-ROI_{n,1} and WIn-ratio-ROI_{n,1} demonstrated moderate to good inter- and intra-reader agreements. At t₂, among the K_{trans}-related parameters, only K_{trans} -ratio-ROI_n and K_{trans} -ratio-ROI_s showed both satisfying inter and intra-reader agreements.

	Early evaluation t₁			Late evaluation t₂	
	Intra-rater agreement (Ra1-1 vs Ra1-2)	Inter-rater agreement (Ra1-1 vs Ra2)		Intra-rater agreement (Ra1-1 vs Ra1-2)	Inter-rater agreement (Ra1-1 vs Ra2)
%change Longest diameter	0,724 (0,552 ; 0,322) *	0,703 (0,521 ; 0,824) *	%change Longest diameter	0,902 (0,811 ; 0,951) **	0,821 (0,655 ; 0,910) **
RECIST _{0→1}	0,828 (0,642 ; 1) **	0,436 (0,124 ; 0,748)	RECIST _{0→2}	0,717 (0,460 ; 0,974) *	0,660 (0,391 ; 0,929) *
%change a x b	0,837 (0,725 ; 0,906) **	0,761 (0,606 ; 0,861) *	%change a x b	0,518 (0,215 ; 0,730)	0,625 (-0,520 ; 0,864)
OMS _{0→1}	0,504 (0,253 ; 0,755)	0,222 (-0,074 ; 0,518)	OMS _{0→2}	0,182 (-0,020 ; 0,384)	0,136 (-0,078 ; 0,350)
%Fibrosis	0,102 (-0,257 ; 0,461)	0,556 (0,215 ; 0,897)	%Fibrosis	0,636 (0,364 ; 0,908) *	-0,424 (-0,685 ; -0,163)
Pattern of fibrosis	0,416 (0,128 ; 0,704)	0,525 (0,272 ; 0,778)	Pattern of fibrosis	0,788 (0,561 ; 1) *	0,276 (-0,685 ; -0,163)
PE-ROI _n	0,885 (0,802 ; 0,934) **	0,957 (0,923 ; 0,976) **	PE-ROI _n	0,740 (0,530 ; 0,865) *	0,891 (0,788 ; 0,946) **
WIn-ratio-ROI _n	0,790 (0,648 ; 0,880) **	0,736 (0,565 ; 0,847) *	WIn-ratio-ROI _n	0,615 (0,342 ; 0,713) *	0,776 (0,584 ; 0,836) **
			K _{trans} -ROI _n	0,338 (-0,510 ; 0,641)	0,751 (0,518 ; 0,882) **
			K _{trans} -ratio-ROI _n	0,776 (0,584 ; 0,886) **	0,615 (0,342 ; 0,793) *
			K _{trans} -ROI _s	0,177 (-0,213 ; 0,521)	0,295 (-0,910 ; 0,606)
			K _{trans} -ratio-ROI _s	0,591 (-0,251 ; 0,802) *	0,799 (0,599 ; 0,906) **

Table 5 : Inter-reader agreement and 95% confidence intervals for relevant measurements, conventional MRI and DCE-MRI parameters at t1 and t2

* indicates parameters with substantial/moderate agreement (κ and $\kappa_w=0.60-0.80$, ICC=0.50-0.75), ** with almost perfect/good agreement (κ and

$\kappa_w > 0.80$, ICC > 0.75)

6. Combination of significant criteria at t_1 to predict response

Due to their poor reproducibility's, none of the conventional MRI criterion were introduced in the multivariate analysis. After dichotomisation of PE-ROI_{n,1} and WIn-ratio-ROI_{n,1} according to the thresholds that were found on ROC analysis and verification of the absence of collinearity between them ($r^2=0.147$), a logistic binary regression was conducted. The model included gender, PE-ROI_{n,1} and WIn-ratio-ROI_{n,1}. When the 3 predictors were considered together, they significantly predicted histologic response ($p=0.004$). The model enabled to explain 38.7% of the variation of the outcome (Nagelkerke- $R^2=0.387$), fit well with the data (Hosmer-Lemeshow test, $p=0.340$), with a diagnostic accuracy of 84.4%. Indeed, only 2/34 (5.9%) PHR were ill classified as good responders. Thus, Se was 94.1%, Sp 54.5%, PPV 86.5% and AUC of ROC curve of the model was 0.836 IC95% (0.677 – 0.994) to detect PHR.

However 5/11 (45.5%) GHR were ill classified as poor responders. None of the 3 predictors alone significantly predicted the histologic response when all were introduced in the model. Table 6 shows the results of the binary logistic regression. Figure 8 shows ROC curve of the model. Finally, after each predictor being dichotomised, the equation of the model was:

$$\log(p/(1-p)) = 0.811 \times (\text{WIn-ratio-ROI}_{s,1}) + 2.085 \times (\text{Gender}) + 1.647 \times (\text{PE-ROI}_{s,1}) - 0.592$$

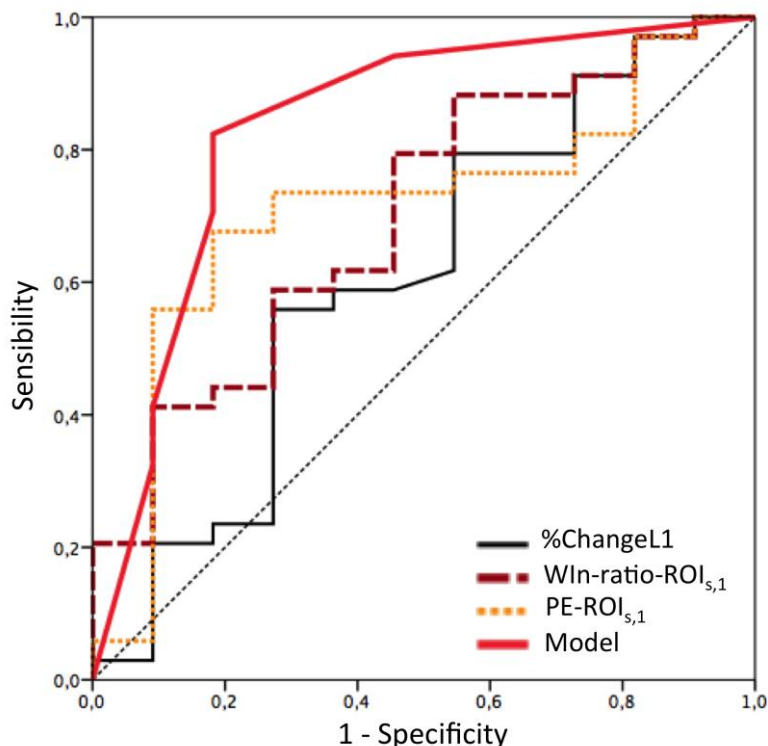


Figure 8. ROC curves at early evaluation of % change of the longest diameter, DCE-MRI predictors alone (WIn-ratio-ROI_{s,1}, PE-ROI_{s,1}) and of the multivariate model.

Table 6 : Synthesis of the Multivariate binary logistic regression results to predict pathologic response at early evaluation t_1 . (A) OR with their 95% IC and p-value, estimated after univariate and multivariate analyses. (B) Patient's classification according to the model. Note that one of the initial 46 patients had too poor quality DCE-MRI₁ to compute the semi-quantitative and quantitative parametric maps and was removed from this analysis. (C) Area under curve of ROC curve of the model, %Change of maximal axis (L1) from t_0 to t_1 , PE-ROI_{s,1} and Win-ratio-ROI_{s,1} with standard error, 95% IC and p-value

A.

	OR - univariate analysis	OR – multivariate analysis
Gender	11 (1.42 ; 124.60) p=0.015 *	8.04 (0.82 ; 79.09) p=0.074
PE-ROI _{s,1}	10.45 (0.198 ; 51.22) p=0.006 **	5.19 (0.76 ; 35.35) p=0.092
Win-ratio-ROI _{s,1}	5.4 (1.17 ; 23.72) p=0.026 *	2.25 (0.38 ; 13.29) p=0.371

B.

	True-PHR	True-GHR	
Model +	32	5	37
Model -	2	6	8
	34	11	45

C.

	AUC	Standard error	95% IC
0%Change-L1	0.608	0.105	(0.403 ; 0.814)
Win-ratio-ROI _{s,1}	0.701	0.090	(0.525 ; 0.876)
PE-ROI _{s,1}	0.711	0.089	(0.536 ; 0.886)
Multivariate Model	0.836	0.081	(0.677 ; 0.994)

7. Particularities of myxoid-round cells liposarcomas response with a-NAC

Our series included 6 myxoid-round cell liposarcomas (M/RC-LPS), which were all considered as PHR after pathological analysis of surgical specimen. In 4 of 6 cases, the pathologists specified that the round cell component had disappeared and that only remained the myxoid component raising the question of how to evaluate pathologic response in M/RC-LPS.

Retrospective analysis of the M/RC-LPS showed a particular imaging pattern of response. Maximal diameter, minimal diameter and volume were not modified between t_0 and t_1 (paired Wilcoxon, $p > 0.05$). Conventional MRI₀ showed well-limited tumour, without peripheral oedema. At t_1 , 2/6 showed small haemorrhage on MRI₁. Fibrosis <50% was reported in 4/6 patients with apparition of either septa, diffuse or peripheral fibrosis. Fatty component also increased suggesting a RE-differentiation with a-NAC.

DCE-MRI₁ thresholds were poorly efficient. PE-ROI_{n,1} was positive in one case. WIn-ratio-ROI_{n,1} was positive in 4 cases. Thus, one male patient had all the three model predictors negative leading to misdiagnosis. In this case, one must note that round cells component was absent on surgical specimen. Figure 9 shows a typical evolution of M-RC LPS treated with a-NAC.

8. Retrospective analysis of ill-classified responses to highlight clues to avoid misclassification (Figure 10).

In order to identify the limits of the multivariate model, we retrospectively analysed the images of the 5 ill-classified true GHR and the 2 ill-classified PHR.

Four of the 5 true GHR did not demonstrate any suggestive sign of a response to treatment at t_1 : neither on conventional MRI₁, nor on DCE-MRI₁. However, these 4 true GHR displayed morphological and perfusion alterations between t_1 and t_2 strongly evocative of a good response: 3/4 turned into entire fibro-necrotic tumours, without arterial phase enhancement, 1/4 remained morphologically poorly unchanged. However, this patient benefited from a DCE-MRI after 4 cycles of a-NAC showing less than 10% of arterial phase enhancement, WIn-ratio-ROI_s and PE-ROI_s under cut-offs. These four cases suggest the possibility of 'late responders to a-NAC' (Figure 11.A). One of the 5 true GHR still demonstrated at t_2 one component with perfusion abnormalities ('Aggressive' time-vs-[Gd] curve, WIn-ratio-ROI_{s,2} = 5.3 mmol.L⁻¹.s⁻¹) (Figure 11.B).

One of the 2 ill classified true PHR was a M/RC-LPS (see section 7. of results for details).

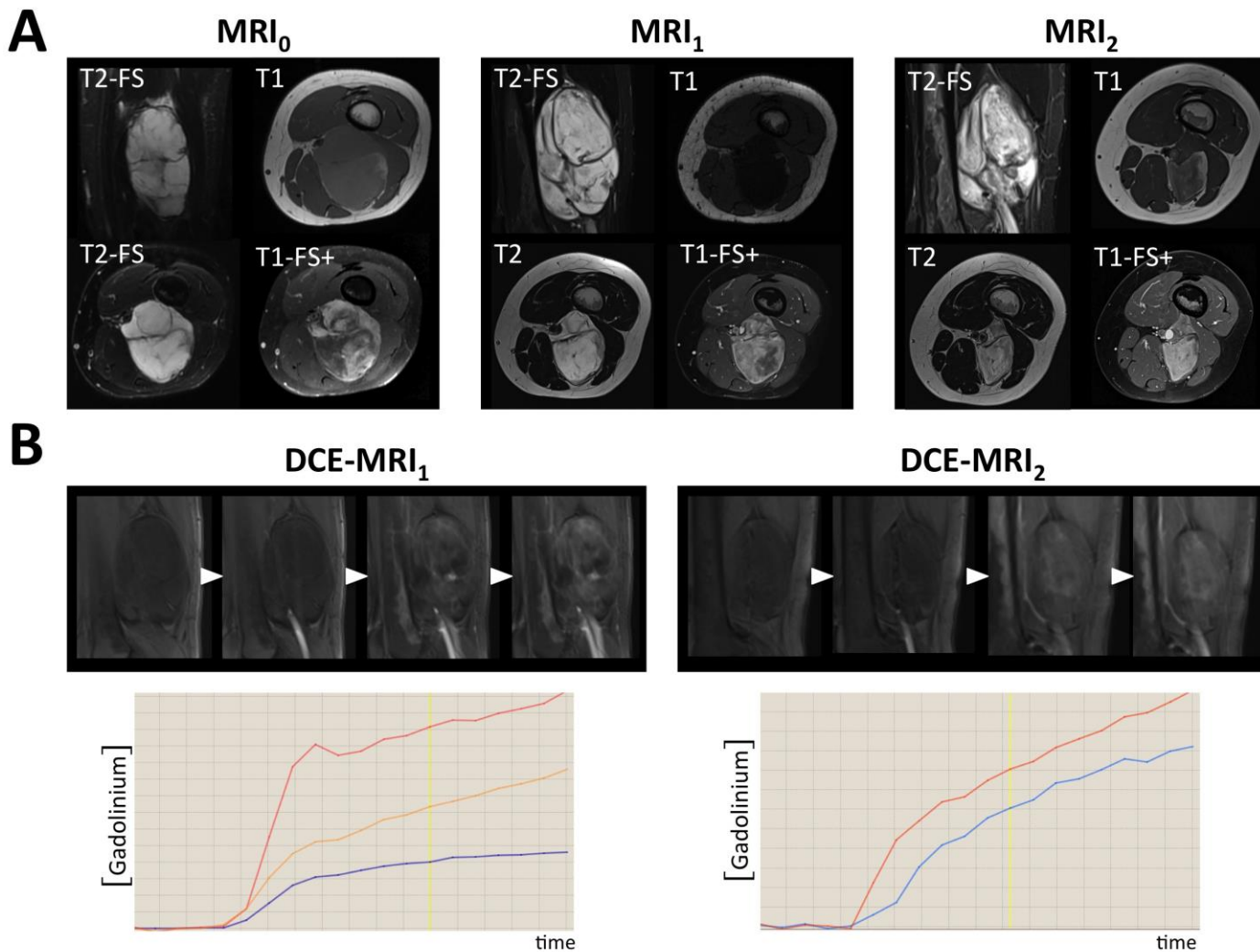


Figure 9. RE-differentiation pattern of response of M/RC-LPS under a-NAC.

(A) shows conventional MRI at each evaluation point. Maximal diameter did not change. Tumour transverse axis tended to decrease. Note the apparition of additional fatty component within tumour periphery (high SI on T1-wi, low SI on post-contrast fat suppressed T1-wi). (B) Selection of DCE-MRI raw images (prior to CA injection and at arterial, venous and late phases), shows patchy venous and late enhancements, with disappearing of some enhanced area on DCE-MRI₂. (C) Curves at early and late evaluation: at t₁, ROI_N-corresponding curve (red) was classified type-1, that is to say 'aggressive' compared with muscle curve (blue). At t₂, the curve was classified type-0. Altogether, DCE-MRI data were compatible with a late good response, but tumour was pathologically classified as PHR because of >10% viable cells despite no round cells.

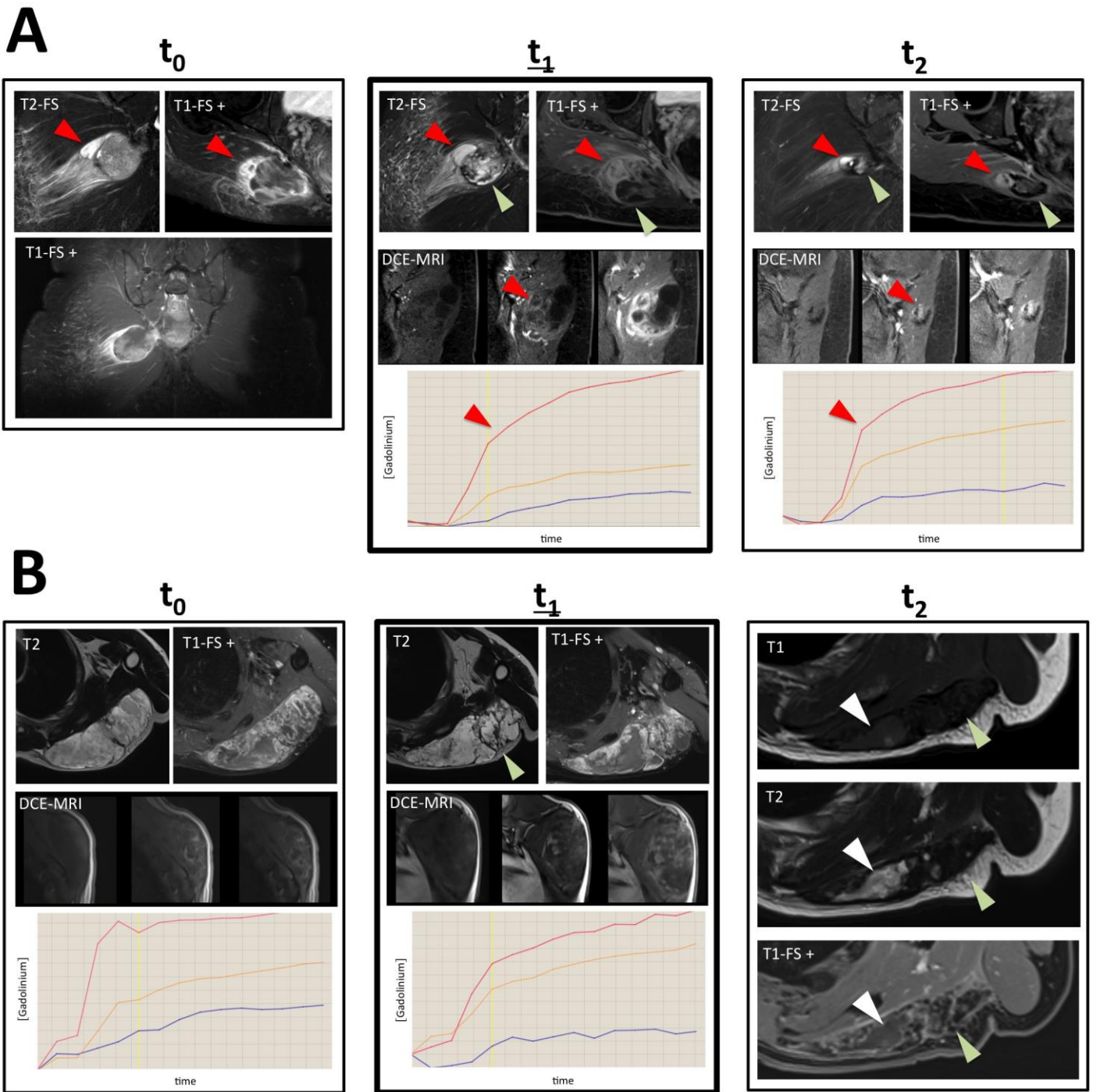


Figure 10. Two cases of ill classified true-good histologic responders for two different reasons.

(A) Is this STS well-responding? Is this a late-late responder? Follow up demonstrates persistence of a tissue nodule with strong and early enhancement (red arrow head and red curve) while the posterior nodule showed fibrotic process followed by retraction (green arrow head)

(B) Is this STS a late responder? At t_1 , rare fibrotic septa appeared. At t_2 , tumour only displayed fibrosis (green arrow head) and necrosis (white arrow head). Pathological analysis reported no residual tumour cells and only fibro-necrotic tissue (note that because of movement artefacts due to breathing, patient was removed from quantitative DCE-MRI studies)

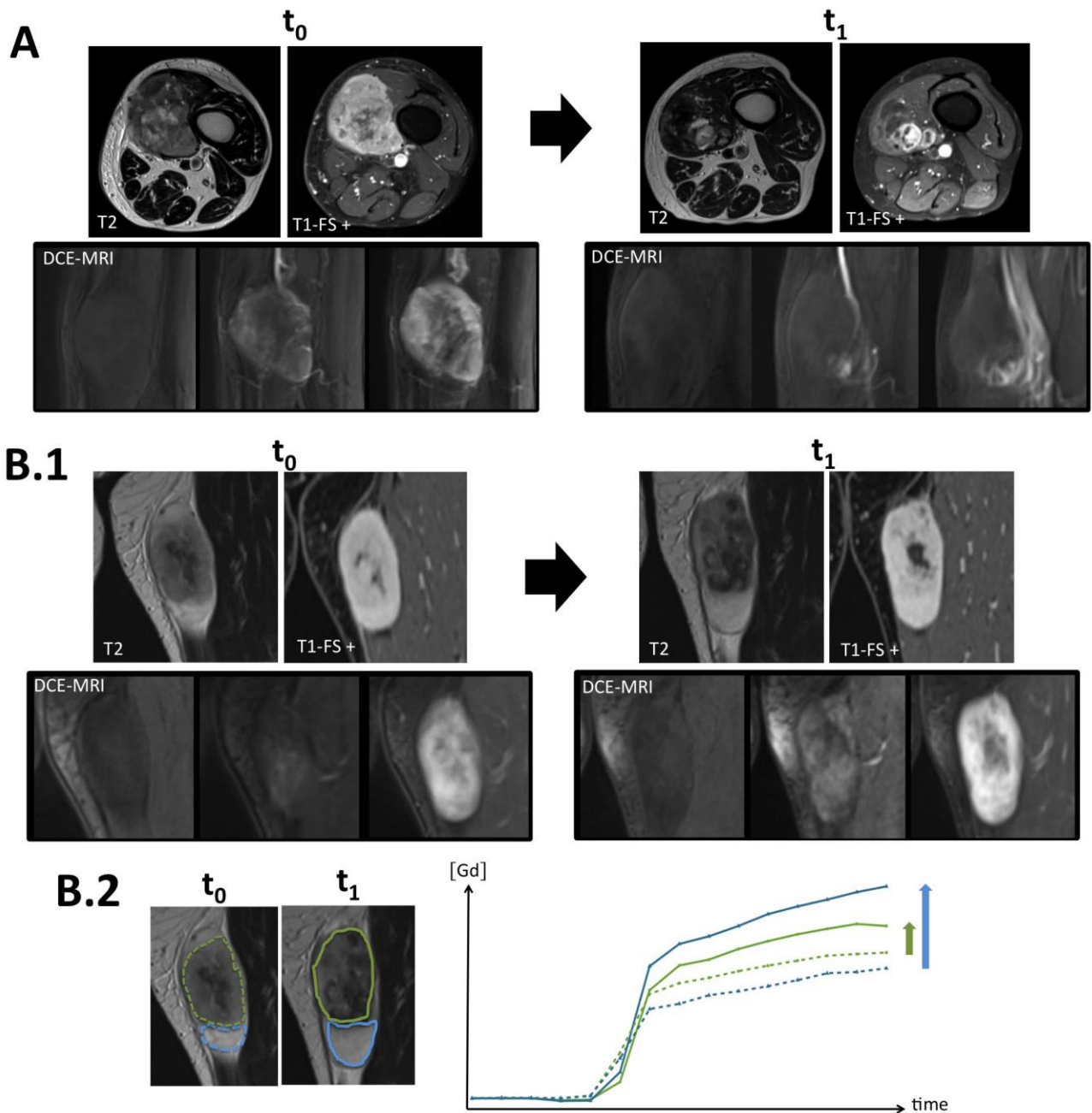


Figure 11. Identification of a-NAC resistant compartment.

(A) show as typical ‘compartmental fibrosis’ pattern of response where only a nodule still displayed early arterial enhancement after two courses of a-NAC. Conventional MRI and DCE-MRI at t_0 did not identify a priori abnormality in the future primary or secondary ‘resistant’ nodule.

(B) shows a another case of ‘compartmental fibrosis’ where the resistant nodule, at its lower part, clearly displayed different features from the rest of the tumour on conventional MRI₀ and DCE-MRI₀. (B.1)

Curvology: Interestingly, this resistant nodule (blue dotted line) was initially slightly less perfused than the rest of the tumour on initial MRI (green dotted line). After 2 cycles of a-NAC (same colour, continuous line), the curves inverted with resistant nodule becoming the most perfused.

9. Multiparametric MRI analysis of a-NAC resistant compartment (Figure 11)

Conventional MRI analysis at t_1 enabled to distinguish 12 patients with a heterogeneous response, called ‘compartmental fibrosis’ because one component clearly exhibited a strong fibrotic response, while at least one another component was absolutely not affected by a-NAC (persistent nodule). One was a GHR and 11/12 were PHR.

Among the 12 cases of compartmental fibrosis at t_1 :

- 2/12 patients had $MRI_0 + DCE-MRI_0$ without any clues for a future persistent nodule (Figure 12.A).
- 9/12 patients only had MRI_0 without any clues on conventional analysis for a future persistent nodule.
- 1/12 patient had a tumour of which $MRI_0 + DCE-MI_0$ demonstrated a different nodule that would grow under a-NAC while the rest of the tumour got fibrotic (Figure 12.B). Interestingly, this component was moderately vascularized compared with the others at t_0 .

10. Correlation between relevant DCE-MRI parameters at t_2 and percentage of viable cell on surgical specimen (Figure 12, table 7)

We believed that one explanation of the failure of our model to correctly classify 45.5% of good responders was due to the lack of criterion to estimate good response, that is to say, to estimate %fibrosis and %necrosis. %Fibrosis estimated on MRI_1 was not reproducible enough to be acceptable in a model.

On another point of view, we hypothesized the ability of the multivariate model to correctly classify 94.1% of poor responders was likely due to the positive relationship between DCE-MRI numeric indices and residual viable cells.

To test this hypothesis, we performed univariate and multivariate linear regressions that took into account the significant criteria to distinguish PHR and GHR at t_2 , prior to surgery. In this part of the study, we also made the assumption that modifications of tumour between t_2 and surgery would remain limited, thus conventional MRI_2 and $DCE-MRI_2$ would be direct reflection of the tumour.

The other aim of this part is to capture the information contained in continuous data (% of viable cell) and lost with dichotomisation (PHR or GHR with a cut-off of 10% of residual viable cells).

Table 8 and figure 13 summarizes the results of univariate and multivariate linear regression between %viable tumour cells on surgical specimen and quantitative possible numeric predictors, beforehand identified as significantly different between GHR and PHR at t_2 . Finally, multivariate analysis demonstrated that $WIn\text{-ratio-ROI}_{n,2}$ and %change of the longest dimension showed significant correlation with % viable tumour cells ($r=0.370$, $p=0.022$ and $r=0.394$, $p=0.029$,

respectively). Together with results at t_1 , this highlights the potential of WIn-ratio-ROI_n as a biomarker of pathological response.

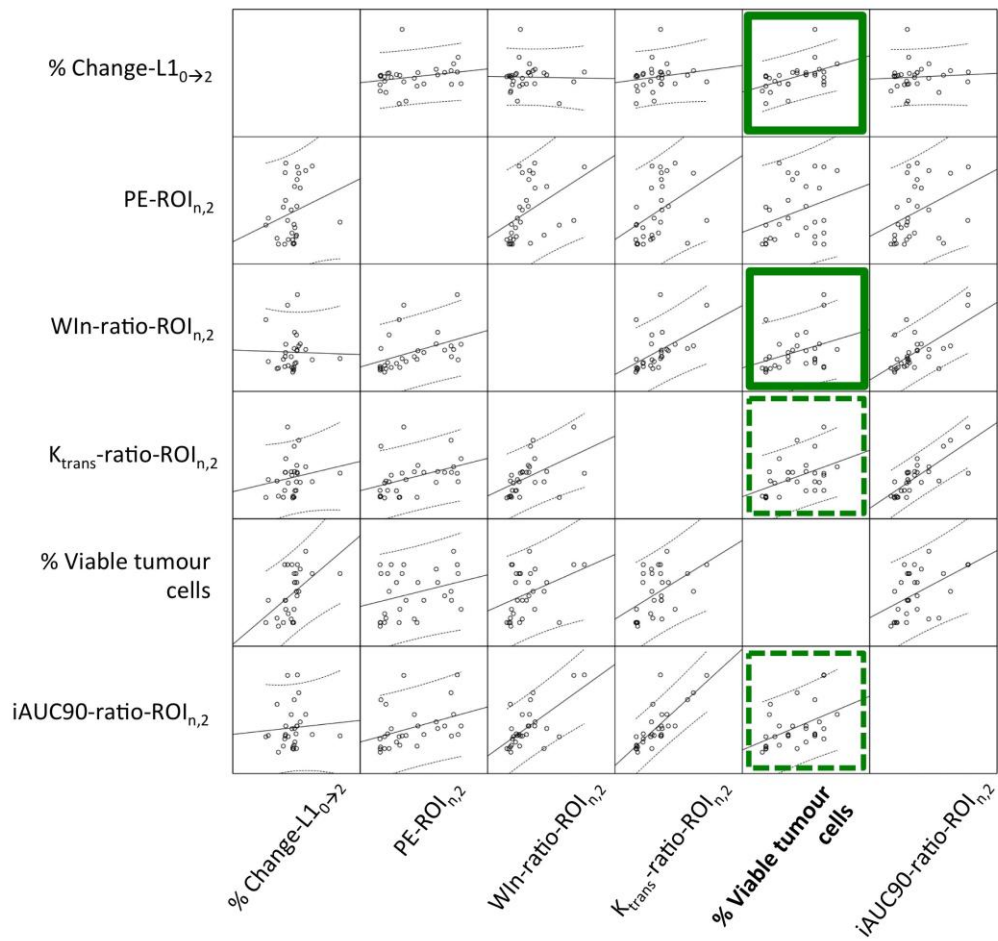


Figure 12. Scatterplot of the continuous variables included in multivariate linear regression model at pre-operative t_2 . (Dotted green line: included variable but not significant when individually considered. Green line: significant correlations on univariate and multivariate analyses.)

Table 7. Uni and Multivariate Linear Regression between relevant continuous variables and % at t₂

	Univariate		Multivariate	
	r	p	r	p
%Change-L1 0→2 (N=32)	0.410	0.020 *	0.370	0.022 *
%Change-‘axb’ 0→2 (N=32)	0.447	0.010 *	–	–
%Change-Volume 0→2 (N=32)	0.347	0.035 *	–	–
Win-ratio-ROI _{n,2} (N=32)	0.489	0.005 **	0.394	0.029 *
iAUC90-ratio-ROI _{n,2} (N=31)	0.570	<0.001 ***	-	-
K _{trans} -ratio-ROI _{n,2} (N=27)	0.562	0.002 **	0.202	0.251
PE-ROI _{n,2} (N=32)	0.287	0.111	–	–

The predictors included in the multivariate analysis were : %change-L1 0→2, Win-ratio-ROI_{n,2} K_{trans}-ratio-ROI_{n,2}.

Their combination significantly predict % of viable tumour cells (ANOVA, F=6.249 ; p=0.002)

Using these 3 predictors simultaneously, adjusted R² was 0.337, meaning that 33.7% of variance of % viable tumour cell could be predicted by their combination

Qualitative criteria, even significantly different between GHR and PHR at t₂, were removed from the analysis because of lack of reproducibility, as well as % Change-‘axb’ 0→2.

Gender and PE-ROI_{n,2} were not significantly correlated with % viable tumour cell and were consequently not included in the model.

iAUC90-ratio-ROI_{n,2} was also removed because of collinearity with other criteria (variance inflation factor = 3.625, tolerance = 0,276).

* : P<0.05 ; ** : p<0.01, *** :p<0.001. All cases with missing data were removed from the analysis.

11. Identification of different peripheral oedema: inflammatory response versus tumour oedema (Figure 13).

We hypothesized that different types of oedema could occur during the NAC. Indeed, at initial evaluation, peripheral oedema is often associated with enhancement after CA injection especially around the tumour, very likely to represent tumour cells spreading and infiltrating surrounding tissue. We called it ‘*tumoral oedema*’.

During the course of a-NAC, we observed a qualitatively different oedema pattern, with a more linear enhancement and a decrease of the extension of pure oedema. This process was seen around fibrotic processes. We called it ‘*peri-granulation inflammation*’ and we hypothesized that it consisted in inflammatory cells infiltrate.

The features ‘presence of an oedema’, ‘increase of fibrosis $t_0 \rightarrow t_1$ ’ and ‘peripheral enhancement’ did not demonstrate significant difference between GHR and PHR at early evaluation t_1 . In order to inventory patients with ‘peri-granulation inflammation’, we combined these three features at t_1 and selected patient with oedema and peripheral enhancement actually occurring around fibrotic process. At t_1 , this combination of features was present in 6 patients, 5/6 GHR and 1/6 PHR.

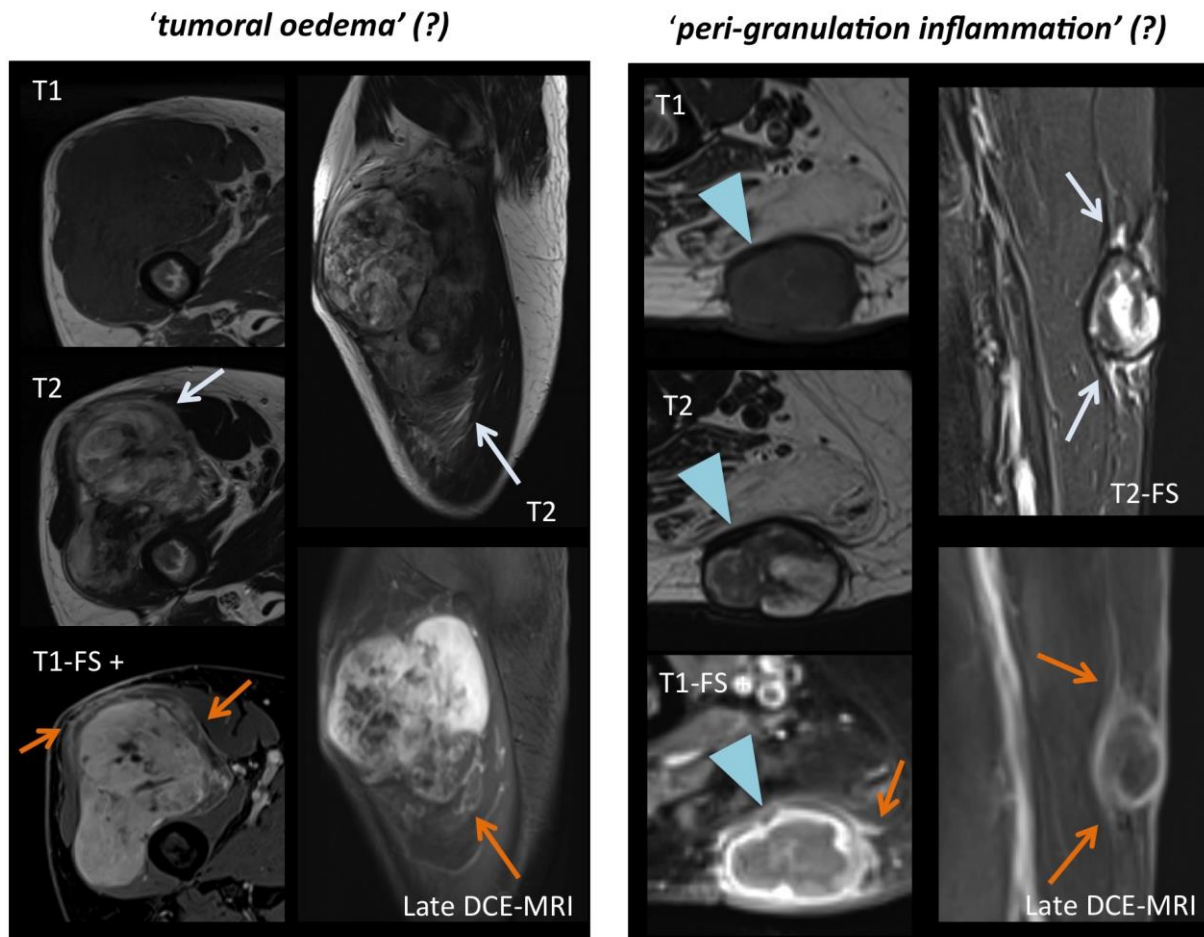


Figure 13. Two different patterns of oedema on conventional MRI.

‘**Tumoral oedema**’ (in a PHR) refers to classically described oedema, with surrounding area of increased SI on T2-wi (black arrow) and focal enhancement of the oedema (orange arrow), suspected to reflect tumour cells deposits in surrounding tissue and hypothesized to have poorer diagnosis.

‘**Peri-granulation inflammation**’ corresponds to less-extended oedema (white arrow on coronal fat suppressed T2-wi). Ill-defined enhancement of the oedema can be seen at the whole tumour surface, abutting a ‘black rim’ of peripheral fibrosis. Pathological analysis on surgical specimen confirmed a good response with clean margins.

*

DISCUSSION

1. Patterns of response under a-NAC

Anthracycline-based NAC leads to a wide range of continuous morphologic and histologic alterations that can be observed and monitored with MRI.

Measures variations are the easiest features to obtain but demonstrate important limits. They occur after angiogenesis and architectural modifications. Size can increase secondary to necrosis, haemorrhage, tumour primary or secondary resistance. Size can decrease due to favourable event such as necrosis or retractile fibrosis, or because one compartment displays excellent response while another is clearly not affected by NAC.

Architectural features on DCE-MRI, despite subjectivity, highlight patterns of response: (i) mainly fibrotic, (ii) mainly necrotic, (iii) fibro-necrotic, and (iv) no apparent response. Interestingly sub-pattern of fibrosis could be discriminated: (i) diffuse, (ii) septa, (iii) peripheral and (iv) compartmental fibrosis. The 'compartmental fibrosis' sub-pattern stresses the hypothesis of primary or secondary a-NAC resistant component within a tumour that mainly favourably responds. However, there is a strong assumption that architectural 'macroscopic' MRI features follow modifications of tumour vascularization, assessed by DCE-MRI.

2. Improvement of early prediction with DCE-MRI

After 2 cycles of a-NAC, semi-quantitative DCE-MRI indices were able to significantly predict a poor histologic response with an excellent sensitivity (94.1%), while variations of longest diameter, bi-dimensional diameters, volume and conventional MRI qualitative analysis and T2-ratio were not significantly different between PHR and GHR, except for estimate of %fibrosis, of which inter and intra-observer reproducibilities were low.

At the end of a-NAC, all the measures, the pattern of fibrosis, several items of qualitative, semi-quantitative and quantitative analyses of DCE-MRI predicted histologic response.

Overall, these results support the idea of a continuum of perfusion, architectural and dimensional alterations.

We believed that integrating the whole information from each modality of evaluation, instead of being exclusive, would improve response prediction.

However, the model (with or without taking into account gender) failed to identify 41.7% (5/12, one of them having poor quality DCE-MRI₁ which was removed from the semi-quantitative and quantitative analyses) true GHR at early evaluation. MRI follow-up of one of these 5 patients demonstrated a 'compartmental fibrosis': one compartment remaining unchanged, questioning in this sole case, the coherence between radiological and pathological results. The other cases

demonstrated features compatible with GHR on late evaluation, highlighting a ‘late responders’ phenotype on MRI (about 33.3% of all GHR).

Occurrence of compartmental fibrosis made us consider the hypothesis of mechanisms of resistance to a-NAC either before (primary resistance) or after the beginning of chemotherapy (secondary resistance).

We wondered if retrospective analysis of MRI₀ and DCE-MRI₀ could have helped to identify imaging features of potential primary resistance and, if yes, which DCE-MRI features would be associated. Only 3 of the 12 patients with compartmental fibrosis underwent both MRI₀ and DCE-MRI₀. Two of them did not demonstrate any evidence of different imaging features at t₀. One tumour initially demonstrated a less vascularized area at the right place of the future persistent nodule. From this observation, one could hypothesize that resistance would come from combination of hypoxia (eventually assessed by PET-CT or PET-MRI or Spectroscopy-MRI) and lower provided dose of chemotherapy

Furthermore, difficulties to detect these resistant components - if truly pre-existing (that is, pre-existing different molecular features) - could also be due to limitations of our MR sequences and analysis methods. Another hypothesis could also be that the nodule secondarily appeared (apparition of molecular heterogeneity after and/or due to a-NAC – secondary resistance).

Further multi-parametric MRI studies could explore in more details these two patterns (compartmental fibrosis and late responders) in order to detect them at initial or early evaluation with better accuracy and to target them for imaging guided biopsy (MRI or fusion Ultrasound-MRI). Sampling and making tumour molecular screening of these sub-groups of STS could potentially identify primary or secondary resistance pathways (and help adjust treatment toward neo-adjuvant radiotherapy or ILP) to NAC, as well as underlying molecular particularities of late responders.

Genomics, transcriptomics, proteomics knowledges and applications in oncology have incredibly raised and, additionally to radiomics analogical approach, imaging must participate to this infatuation by looking for every deviance to expected results.

3. Correlations between % viable tumour cells and DCE-MRI indices

In an attempt to evaluate the information lost by dichotomising variables, we demonstrated that % of viable tumour cells was positively correlated with several DCE-MRI metrics, notably, in the multivariate analysis, with WIn-ratio-ROI_t. All the variations of measures also demonstrated significant correlations. If confirmed, these results could help treatment decision such as surgical planning, additional other treatment (radiotherapy, ILP)

4. M/RC-LPS: how to evaluate response to treatment?

Both radiological and pathological analyses were limited to estimate response in these cases. All were classified as PHR. However, in 4 cases, pathologists noticed they did not find round cells among the numerous residual tumour cells. MRI and DCE-MRI did not report tumour shrinkage or necrosis, as it has been described with Trabectedin (Grosso et al., 2007; Hollebecque et al., 2010). On the contrary, tumours tended to remain stable at early evaluation. Later, at t_2 , we found size decrease with apparition of fatty component and some haemorrhagic foci as well as DCE-MRI parameters decrease. These responses suggested a re-differentiation pattern, similar to the ‘non dimensional tumour response’ pattern with Trabectedin, proposed by Sanfilippo and Casali (San Filippo et Casali, 2013). In their review, the authors distinguished this pattern from ‘tumour shrinkage’ pattern. They explained its occurrence by a specific activity of Trabectedin that would target and block FUS-CHOP transcript leading to adipogenic differentiation. Thus, our observations suggest that this activity may also be possible with anthracycline-based NAC.

Work in progress

→ Conventional MRI and DCE-MRI comparisons of imaging response of local cases (Bergonie institute) of M/RC-LPS under neoadjuvant Trabectedin (n=6) and Anthracycline-based chemotherapy (n=9) with available final pathological analysis and surgical specimen samples.

We will investigate the similarity of: (i) the ‘*non dimensional tumour response*’ and (ii) targeting of FUS-CHOP transcript with a-NAC

Nonetheless, assessment of percentage of round cells (%RC) at diagnosis is challenging. >5 %RC is associated with poorer outcome, but is quantified on a small micro-biopsy that only estimated a very small amount of the tumour (Fiore et al., 2007; Haniball et al., 2011). Recent studies have tried to address this issue (Gimber et al., 2017) but results are biased because the gold standard was %RC on surgical specimen AFTER neoadjuvant treatment and MRI was performed prior.

Thus, conventional, functional, texture MRI features of M/RC-LPS associated with poor prognosis (and supposed to reflect initial %RC) remain mainly unknown.

Prospects

→ *There is a need for collaborative retrospective multicentric study to investigate the prognostic value of MRI radiomics-based indices enriched with bioclinical data that would predict disease free survival and overall survival of M/RC-LPS.*

For those patients who underwent direct curative surgery without neoadjuvant treatment, correlations between conventional MRI, DCE-MRI, MRI-radiomics metrics and %RC should be assessed.

5. Patterns of peripheral oedema and immune reactions during a-NAC

STS surrounding oedema, prior to any treatment, is a well-known phenomenon. It is said to correspond to reactive zone, beyond tumour periphery or pseudocapsule, made of neovascularization, oedema and satellite tumour cells, partly responsible for tumour local recurrence (Enneking et al., 1981; White et al., 2005; Hanna et al., 1991).

Looking at pre, per and post-therapeutic MRIs, we identified another original pattern of surrounding oedema evolution, which we called ‘peri-granulation inflammation’. We defined it as a persistent but decreased surrounding area of high SI on T2-wi, T2-FS-wi or DP-FS-wi associated with ill-limited peripheral enhancement adjacent to a fibrotic process. In case of peripheral fibrosis pattern, this enhancement was located on each side of the fibrotic coating (displaying low SI on T1-wi, T2-wi), giving a ‘black-rim’ aspect. This pattern was seen in 6/46 patients: 1 PHR and 5 GHR.

This ‘black rim’ looked different from the classical pseudocapsule, due to compression and atrophy of peripheral tissue, because it was initially absent and was observed in superficial tissue where no muscle tissue could have been pushed and compressed.

We hypothesize that this oedema may reflect a favourable immune inflammation leading to fibrosis of the tumour. Further studies to investigate its precise nature, its association with histological or molecular features, and its prognostic impact are required.

Work in progress

→ At t_2 , we also looked for the cases also demonstrating ‘peri-granulation inflammation’ and ‘tumoral edema’.

→ We are going to analyse the HES slides that sampled the tumour margins on surgical specimen to look for which type of cellular infiltrate was surrounding the tumour, either inflammatory cells (and which subtype of cells) or tumour cells

→ If histology actually confirms different cells infiltrate, we will investigate the tumour surrounding tissue with multiparametric imagings to better characterize its features.

6. Limits

Our study has several limits:

6.1. This is a retrospective study, but this step is mandatory before planning prospective study in oncology.

6.2. This is a single-centre study, but one aim of our work is to obtain an uniformly-treated population. Anthracycline-based NAC is becoming the reference NAC, performing better than histotype-tailored NAC but few centres actually prescribed it alone, without radiotherapy (Gronchi et al., 2017).

6.3. Furthermore, our patient population (N=46) could appear small but, to the best of our knowledge, this is the largest effective to evaluate MRI +DCE-MRI values to predict histologic response.

6.4. One could argue that our patient population is made of different histotypes. We pooled together different high-grade STS due to their rarities, their inclusion in same clinical trials, leading to same treatment, same follow-up in same sarcoma reference.

Alveolar soft part sarcomas, known to be hyper vascularized, were naturally excluded because the reference treatment consists in anti-angiogenic therapy (Reichardt et al., 2003; Kummar et al., 2013)

Larger studies would have to perform multivariate analysis taking into account histotypes, notably, M/RC-LPS.

6.5. The treatment response was evaluated in this study using % viable tumour cell on pathological analysis of surgical specimen by analogy with osteosarcomas (Salzer-Kuntschik et al., 1983). Other centres use % of necrosis or mitotic count (Andreou et al., 2015) as a markers of response. Recent ASCO communication demonstrated that this criterion with this cut-off was also predictive of overall survival (Cousin et al., 2017). A consensual definition appears crucial.

The method of quantification, namely a percentage of tumour volume without taking in account the absolute tumour volume, could be questionable. We observed cases where component that were compatible with viable tumour on MRI, strongly decreased. Yet, these cases were considered as PHR because the necrosis got cleaned between t_1 and t_2 , and because fibrosis tended to retract.

Response of massively necrotic tumours is also difficult to estimate for both radiologists and pathologists. On a radiological point of view, the positioning of ROI_N on the first enhanced component on DCE-MRI sequence is tricky or even unfeasable, some tumours only exhibiting a thin peripheral CA uptake. On a pathologist point of view, liquefied necrosis and cystic compartment are often cored, evacuated during the fresh state step and excluded from the final percentages, leading to over-estimation of % fibrosis and % viable cells, a case that we encountered in this study. A solution could be to combine MRI estimation of necrosis and pathological analysis. Monsky et al. proposed a semi-automated MRI method to segmentate necrosis with good correlation (Monsky et al., 2012).

Finally, a 5 μ m slice is used to sample a volume of 1cm³, chosen because it seems to be representative at the macroscopy step, relying on subjectivity of the pathologist and of the technician.

6.6. Our method to analyse conventional MRI, qualitative DCE-MRI and to place ROI_S, ROI_N and ROI₃ for the semi-quantitative and quantitative analyses also relies on subjectivity. Nonetheless, when used by specialized radiologists from a sarcoma reference centre, DCE-MRI inter- and intra-

observers agreements were acceptable, except for model based indices, and in the range of %change of longest diameter, on which is based on RECIST1.1. On a practical point of view, working on average values from manually placed ROI represents the easiest and less time-expensive way to obtain information. We believed than in the setting of future clinical trials that would include DCE-MRI in imaging evaluation, this method could be of interest.

6.7. We decided to evaluate ratio of the indices in addition to their absolute values because tumour location, depth, arterial input function, MRI coils greatly differed in our population study. The % of tumour volume with enhancement at arterial phase has demonstrated ability to predict response in prior studies, reason why we aimed at specifically studying its DCE-MRI properties in our ROI-based analysis (Soldatos et al., 2016; Van Rijswijk et al., 2003).

6.8. We decided not to analyse DCE-MRI parameters related to the late part of the acquisitions, that is wash out and return transfer from tissue to plasma, because our DCE-MRI protocol only last 3mn30s.

6.8. DCE-MRI is a complex method that required trained team of technicians and radiologists to respect the technical recommendations of RSNA QIBA alliance. Nonetheless, we had to remove (18.8%) 19/101 quantitative DCE-MRI from the study: 7 because of poor quality (movements, inadequate arterial input function) and 12 because of mismatch between raw-data, semi-quantitative metrics and K_{trans} (Figure 14). One reason could be inadequacy of Tofts-Kety model to estimate STS vascularization, especially for distant and strongly arterialized location, but also to accumulations of factors contributing to biases (temporal downsampling, too short total scan time AIF and T1-mapping of poor quality, low signal-to-noise ratio, B1 inhomogeneity, partial volume effect, errors in haematocrit, distance between tumour and arterial input, injection rate...) (Lavini, 2015; Rukat et al., 2015).

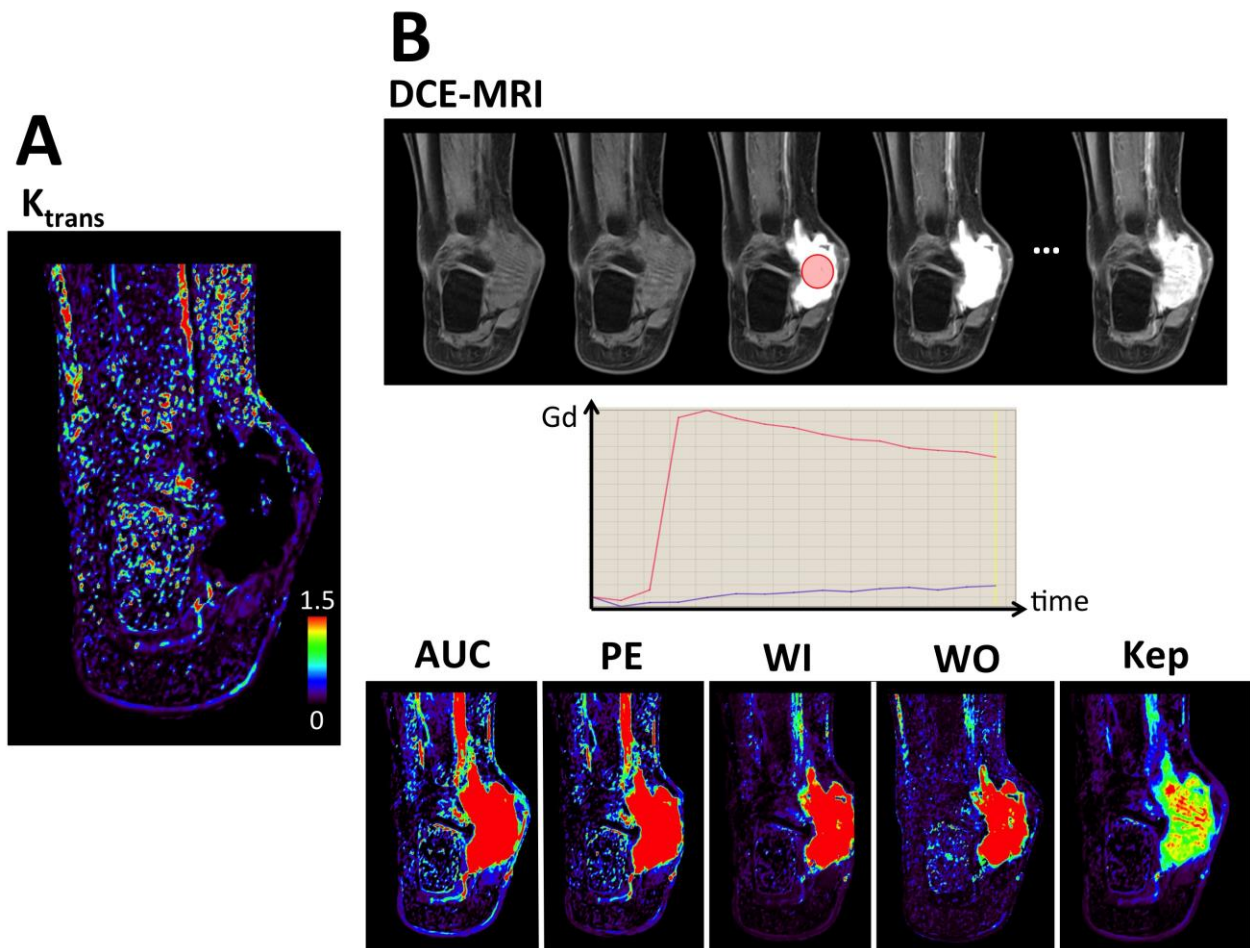


Figure 14. K_{trans} mismatch. (A) K_{trans} map after applying Tofts-Kety model: a 0 value was attributed to each voxel within the tumour (deep+superficial grade III synovialosarcoma of the intern side of the right ankle). (B) However, the raw data, the curve and all the other maps were coherent with an entirely hyper-vascularized tumour (100% of tumour volume enhanced at the first volume acquisition following CA injection). We believe that miscalculation was due to the combined effect of massively hyper-vascularized effect at distant, under-sampling (temporal resolution = 8-9s) and poorly perfused distal location.

6.9. Another limitation is the lack of initial DCE-MRI₀ acquisition for each patient. After control quality, % changes of DCE-MRI indices from t_0 to t_1 were estimable in 21 patients for semi-quantitative analysis (5 GHR and 16 PHR), and 17 patients for quantitative analysis (4 GHR and 13 PHR). Therefore, no conclusion could be drawn from differences between GHR and PHR at t_0 and from t_0 to t_1 . Difference at t_1 may probably be present at pre therapeutic evaluation

6.10. At t_2 evaluation, we found that DCE-MRI₂ indices correlated well with % viable cells suggesting that DCE-MRI would reflect the viable cells component. However, DCE-MRI indices would probably not help to provide a % viable cells at any instant because evolution of % viable cells as a function of days since beginning of NAC probably does not follow a linear function. Here, we did not look for estimators of fibro-necrotic processes but directly to estimators of viable cells, because classification as PHR and GHR relies on their percentage.

Thus, in addition to the proposal of late responders, the lack of estimators of fibrosis and necrosis could explain the limits of our strongly perfectible model. Nonetheless, even imperfect, our goal to demonstrate the potentiality of DCE-MRI indices has been reached.

7. Prospects

7.1. Validation of the semi-quantitative DCE-MRI₁ criteria on external cohort

The thresholds of the two DCE-MRI₁ indices need to be validated before being included in clinical trials design. DCE-MRI lacks of test-retest reproducibility, remains technically challenging, and is very sensitive to conversion of SI to gadolinium chelates concentration. To do so, we are currently assessing their diagnostic performance on a retrospective cohort, with images acquisition made on our previous 1.5-T MR-system. We are also prospectively assessing it on a prospective cohort on our current MR-system through an ancillary study of the Neosarcomics clinical trial (NCT02789384)

Work in progress

→ *Retrospective validation: Data are currently being analysed (N= 25 with same inclusion criteria). Acquisition were performed on our previous 1.5T MR-system between 2007 and 2012.*

Future work

→ *Prospective validation will be performed once Neosarcomics trial inclusion will end and once pathological analysis on all surgical specimens will be available*

7.2. Potential therapeutic consequences of current results

Our results show that a significant proportion of GHR could be mistaken as PHR with RECIST1.1, OMS, volume variation, MRI and DCE-MRI at early evaluation, as well as the existence of a late responders profile on imaging. Current knowledge is not strong and reliable enough to stop neoadjuvant treatment after early evaluation, but rather to perform an intermediate evaluation after 4 cycles. Identification of potential PHR at t₁ could also lead to MRI-guided biopsy in order to sample the residual tumour and screen potential targetable molecular pathways. In case of late responders, this screening could help to identify different pathways of response to a-NAC.

7.3. Moving beyond pathological analysis: towards a radio-pathological evaluation of response?

First, to overcome the under and over estimation of necrosis, fibrosis and residual viable cells, we believe that the post-operative assessment should be consensually made by radiologists and pathologists.

Prognosis impact of multi-parametric MRI should be assessed, alone, and integrated with the whole potential other predictors. Herein, with the oldest case being surgically treated at the end of 2012, the latest at the beginning of 2017, we do not have the necessary hindsight to estimate the prognostic value of each MRI and DCE-MRI indices of the tumour and its periphery.

7.3. Technical optimisation for DCE-MRI

Arterial spin labelling (ASL) is MRI sequence of which the aim is to perform perfusion MRI with endogenous tracers instead of intravenously injected exogenous CA and does not rely on mathematical conversion of SI. It consists in the labelling of arterial spins with a radiofrequency pulse associated with a magnetic field gradient before they arrive in the acquisition volume and secondarily spread within its vessels and tissue. To our knowledge, ASL has not been used to study soft tissue tumours but recent publications has demonstrated its feasibility for musculoskeletal application (Partovi et al., 2015).

7.4. Adding other ‘metrics’ to improve prediction

Other functional quantitative imaging modalities could bring additional values: 18-FDG PET CT scan (Benz et al., 2008; Benz et al., 2009; Hermann et al., 2012; Evilevitch et al., 2008) and spectroscopy MRI (Zhang et al., 2016), elasto-MRI, diffusion-weighted images (Soldatos et al., 2016). In addition, instead of classical ROI-averaging analyses that loose the information about tumour heterogeneity, texture and shape analyses, both parts of ‘radiomics’, could identify new numeric biomarkers. Radiomics refers to the extraction of several quantitative indices, which may not perceptible by radiologist’s eyes, within digital images from any imaging modality. Texture metrics estimate heterogeneity, derived from histogram, co-occurrence matrices, fractal analysis, Minkowski functional... Shape metrics estimate sharpness, compactness, sphericity, edge... These metrics can be combined and correlated with classical radiological semantic assessment (for instance, peri-tumoral edema, pattern of enhancement after injection, speculation...) and with other patient demographics, pathological (from initial biopsy) or molecular data (genomics, transcriptomics, proteomics) in order to finally build signature for tumour diagnosis, tumour aggressiveness, tumour sensibility to specific treatment, patient prognosis. Radiomics approach can be applied on the whole tumour, on tumour sub-compartments, on surrounding tissue and on apparently healthy tissue (Limkin et al., 2017; Gillies et al., 2016; Kumar et al., 2012; Lamblin et al., 2012).

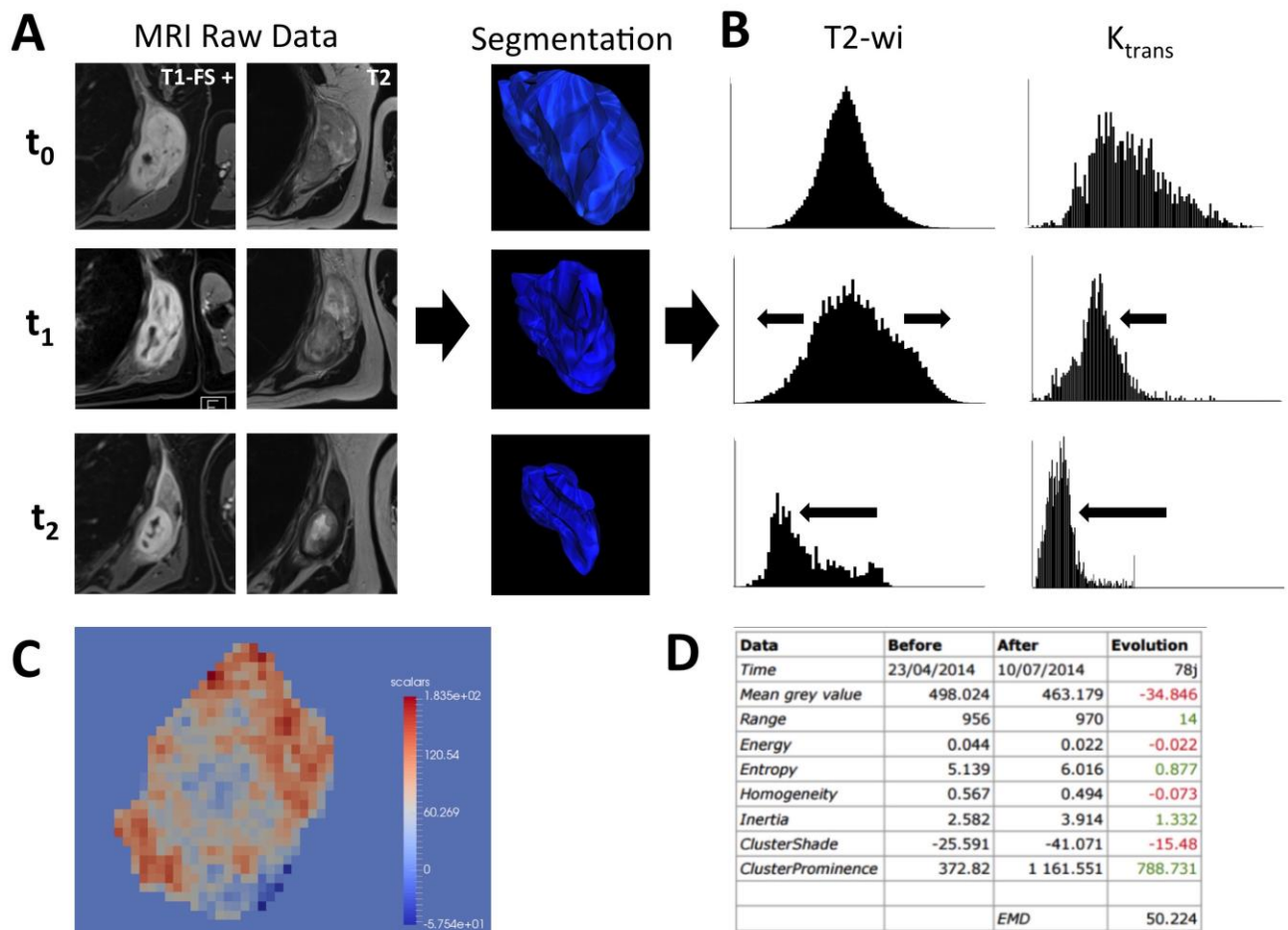


Figure 15. Radiomics process applied to a STS (grade III UPS) under a-NAC. (A) displays the MRI data sets : t_0 : prior to treatment, t_1 : at early evaluation after two cycles of a-NAC and t_2 : at late pre-surgery evaluation (only two sequences among the whole protocole are shown here for the purpose of this figure, that is to say : static T1 fat-Sat weighted images (wi) post-contrast agent injection and T2-wi). (B) shows the semi-automatically segmented volume, on which shape analysis will be performed. This volume is propagated on co-registered MRI, diffusion weighted MRI, dynamic contrast enhanced MRI maps, 18-FDG-PET CT images in order to perform 1st order, 2nd order and higher order radiomics analyses, alone, combined between them and finally with clinical and biological data. (C) shows an example of histogram based analysis on T2-wi and K_{trans} maps demonstrating increased T2 heterogeneity reflecting oedema, fibrotic and necrotic processes already viewable measurable at t_1 (throughg texture indices) as well as decreased K_{trans} heterogeneity, reflecting the reduction of tumour vascularization, which is even more marked at late evaluation. (C) exhibits a representation of gradient-related parameter superimposed on axial slice of the tumour, in order to evaluate NAC-resistant compartment in a sub-region analysis. (D) shows a example of radiomics indices that varied from t_0 to t_1 .

Texture analysis to identify fibrosis and necrotic pattern (Figure 15)

Work in progress

→ *Texture analysis (1st order and 2nd order statistics, taking into account MRI qualitative features and clinical data), with machine learning approach, on T2 sequences is currently being performed (N =90) in order to identify numeric indices at t_1 that are correlated with histologic response and prognosis. MRIs from 60 patients are being processed to investigate the value of changes of the indices from t_0 to t_1 .*

→ *Patients who also benefited from MRI at t_2 will help to build a mathematical model to predict morphometrical local evolution. Patients from Neosarcomics trial will be included in a validation study.*

→ *30 patients from the ongoing texture study are also part of this present DCE-MRI study. We will investigate, after selection and/or creation of composite indices, if additional relevant texture features could improve the prediction model for histologic response.*

Prospects

→ *Ancillary study from Neosarcomics is planned to build a radiomics-based signature for prognosis, prediction of treatment response and identification of radiomics phenotypes correlated with targetable molecular alterations.*

Conclusion

DCE-MRI has been insufficiently studied to assess STS response under NAC. Overall, our results demonstrate potential early predictors of response among DCE-MRI numeric indices, prior to size variation, RECIST1.1 or OMS, this with acceptable reproducibility. Additionally, MRI could help to identify resistant tumours, late responders, original de-differentiation pattern in M/RC-LPS and potential immune inflammation surrounding good responders, requiring further radio-pathological correlations studies. Prospective multicentre studies are required for validation.

*

REFERENCES

- Alic L, van Vliet M, Veenland JF, et al. Regional heterogeneity changes in DCE-MRI as response to isolated limb perfusion in experimental soft-tissue sarcomas. *Contrast Media Mol Imaging*. 2013;8(4):340-9.
- Andreou D, Werner M, Pink D, et al. Prognostic relevance of the mitotic count and the amount of viable tumour after neoadjuvant chemotherapy for primary, localised, high-grade soft tissue sarcoma. *Br J Cancer* 2015;112:455–60.
- Bahri S, Chen JH, Yu HJ, et al. Can dynamic contrast-enhanced MRI (DCE-MRI) predict tumor recurrence and lymph node status in patients with breast cancer? *Ann Oncol*. 2008;19(4):822-4.
- Benjamin RS, Choi H, Charnsangavej C, et al. We should desist using RECIST, at least in GIST. *J Clin Oncol*. 2007;25(13):1760-4.
- Benz MR, Allen-Auerbach MS, Weber WA, et al. Combined assessment of metabolic and volumetric changes for assessment of tumor response in patients with soft-tissue sarcomas. *J Nucl Med*. 2008 ;49 :1579-1584.
- Benz MR, Czernin J, Alen-Auerbach MS, et al. FDG-PET/CT imaging predicts histopathologic treatment responses after the initial cycle of neoadjuvant chemotherapy in high-grade soft tissue sarcomas. *Clin Cancer Res* 2009 ;15 :2856-2863.
- Canter RJ, Martinez SR, Borys D et al. Radiographic and histologic response to neoadjuvant radiotherapy in patients with soft tissue sarcoma. *Ann Surg Oncol*. 2010;17(10):2578-84.
- Choi H, Charnsangavej C, Benjamin RS, et al. Correlation of computed tomography and positron emission tomography in patients with metastatic gastrointestinal stromal tumor treated at a single institution with imatinib mesylate: proposal of new computed tomography response criteria. *J Clin Oncol*. 2007;25(13):1753-9.
- Coindre JM, Nguyen BB, de Mascarel A, et al. Modifications histologiques après chimiothérapie des sarcomes des tissus mous de l'adulte [Histological changes after chemotherapy of soft tissue sarcomas in the adult]. *Ann Pathol*. 1985;5(2):95-9.
- Cousin S, Crombé A, Italiano A, et al. Clinical, radiological and genetic features, associated with the histopathologic response to neoadjuvant chemotherapy (NAC) and outcomes in locally advanced soft tissue sarcoma (STS) patients (STS). *Journal of Clinical Oncology* 2017 35 :15_suppl, 11014-11014
- DCE MRI Technical Committee. DCE MRI Quantification Profile, Quantitative Imaging Biomarkers Alliance. Version 1.0. Reviewed Draft. QIBA, July 1, 2012. Available from http://rsna.org/QIBA_.aspx
- Del Grande F, Subhawong T, Fayad LM, et al. Detection of soft-tissue sarcoma recurrence: added value of functional MR imaging techniques at 3.0 T. *Radiology* 2014;271(2):499-511.
- Dingemans AM, de Langen AJ, Groen HJ, et al. First-line erlotinib and bevacizumab in patients with locally advanced and/or metastatic non-small-cell lung cancer: a phase II study including molecular imaging. *Ann Oncol*. 2011;22(3):559-66.
- Dyke JP, Panicek DM, Ballon D, et al. Osteogenic and Ewing sarcomas: estimation of necrotic fraction during induction chemotherapy with dynamic contrast-enhanced MR imaging. *Radiology* 2003;228(1):271-8.
- Egmont-Petersen M, Hogendoorn PC, Reiber JH, et al. Detection of areas with viable remnant tumor in postchemotherapy patients with Ewing's sarcoma by dynamic contrast-enhanced MRI using pharmacokinetic modeling. *Magn Reson Imaging*. 2000;18(5):525-35.

Eisenhauer EA, Therasse P, Verweij J, et al. New response evaluation criteria in solid tumours: revised RECIST guideline (version 1.1). *Eur J Cancer*. 2009;45(2):228-47.

Enneking WF, Spanier SS, Malawer MM. The effect of the Anatomic setting on the results of surgical procedures for soft parts sarcoma of the thigh. *Cancer* 1981;47(5):1005-22.

Evilevitch V, Weber WA, Tap WD, et al. Reduction of glucose metabolic activity is more accurate than change in size at predicting histopathologic response to neoadjuvant therapy in high-grade soft-tissue sarcomas. *Clin Cancer Res*. 2008;14:715-720.

Fiore M, Grosso F, Gronchi A, et al. Myxoid/round cell and pleomorphic liposarcomas: prognostic factors and survival in a series of patients treated at a single institution. *Cancer* 2007;109(12):2522-31.

FDA+NIH Biomarker Working Group. BEST (Biomarkers, EndpointS, and other Tools) resource. NCBI <http://www.ncbi.nlm.nih.gov/books/NBK326791>. 2016

Gillies RJ, Kinahan PE, Hricak H. Radiomics: Images Are More than Pictures, They Are Data. *Radiology* 2016;278(2):563-77.

Gimber LH, Montgomery EA, Fayad LM, et al. MRI characteristics associated with high-grade myxoid liposarcoma. *Clin Radiol*. 2017;72(7):613.e1-613.e6.

Gronchi A, Ferrari S, Casali PG, et al. Histotype-tailored neoadjuvant chemotherapy versus standard chemotherapy in patients with high-risk soft-tissue sarcomas (ISG-STSS 1001): an international, open-label, randomised, controlled, phase 3, multicentre trial. *Lancet Oncol*. 2017;18(6):812-822.

Grosso F, Jones RL, Casali PG, et al. Efficacy of trabectedin (ecteinascidin-743) in advanced pretreated myxoid liposarcomas: a retrospective study. *Lancet Oncol*. 2007;8(7):595-602.

Guillou L, Coindre JM, Costa J, et al. Comparative study of the National Cancer Institute and French Federation of Cancer Centers Sarcoma Group grading systems in a population of 410 adult patients with soft tissue sarcoma. *J Clin Oncol*. 1997;15(1):350-62.

Hahn OM, Yang C, Stadler WM, et al. Dynamic contrast-enhanced magnetic resonance imaging pharmacodynamic biomarker study of sorafenib in metastatic renal carcinoma. *J Clin Oncol*. 2008;26(28):4572-8.

Haniball J, Sumathi VP, Grimer RJ, et al. Prognostic factors and metastatic patterns in primary myxoid/round-cell liposarcoma. *Sarcoma*. 2011;2011:538085.

Hanna SL, Fletcher BD, Parham DM, Bugg MF. Muscle edema in musculoskeletal tumors: MR imaging characteristics and clinical significance. *J Magn Reson Imaging*. 1991;1(4):441-9.

Hanna SL, Parham DM, Fletcher BD, et al. Assessment of osteosarcoma response to preoperative chemotherapy using dynamic FLASH gadolinium-DTPA-enhanced magnetic resonance mapping. *Invest Radiol*. 1992;27(5):367-73.

Herrmann K, Benz MR, Czernin J, et al. 18-FDG-PET/CT imaging as an early survival predictor in patients with primary high grade soft tissue sarcomas undergoing neoadjuvant therapy. *Clin Cancer Res* 2012;18:2024-2031.

Hollebecque A1, Adenis A, Penel N, et al. Inadequacy of size-based response criteria to assess the efficacy of trabectedin among metastatic sarcoma patients. *Invest New Drugs*. 2010;28(4):529-30.

Huang W, Beckett BR, Ryan CW, et al. Evaluation of Soft Tissue Sarcoma Response to Preoperative Chemoradiotherapy Using Dynamic Contrast-Enhanced Magnetic Resonance Imaging. *Tomography*. 2016;2(4):308-316.

Issels RD, Lindner LH, Hohenberger P, et al.; European Organisation for Research and Treatment of Cancer Soft Tissue and Bone Sarcoma Group (EORTC-STBSG); European Society for Hyperthermic Oncology (ESHO). Neo-adjuvant chemotherapy alone or with regional hyperthermia for localised high-risk soft-tissue sarcoma: a randomised phase 3 multicentre study. *Lancet Oncol.* 2010;11(6):561-70.

Jackson A, O'Connor JP, Parker GJ, Jayson GC. Imaging tumor vascular heterogeneity and angiogenesis using dynamic contrast-enhanced magnetic resonance imaging. *Clin Cancer Res.* 2007;13(12):3449-59.

Jarnagin WR, Schwartz LH, Kemeny N, et al. Regional chemotherapy for unresectable primary liver cancer: results of a phase II clinical trial and assessment of DCE-MRI as a biomarker of survival. *Ann Oncol.* 2009;20(9):1589-95.

Le Grange F, Cassoni AM, Seddon BM. The significance of size change of soft tissue sarcoma during preoperative radiotherapy. *EJSO* 2014;40:394e401.

Kluza E, Rozeboom ED, Beets-Tan RG, et al. T2 weighted signal intensity evolution may predict pathological complete response after treatment for rectal cancer. *Eur Radiol.* 2013;23(1):253-61.

Kumar V, Gu Y, Gillies RJ, et al. Radiomics: the process and the challenges. *Magn Reson Imaging.* 2012;30(9):1234-48.

Lambin P, Rios-Velazquez E, Aerts HJ, et al. Radiomics: extracting more information from medical images using advanced feature analysis. *Eur J Cancer.* 2012;48(4):441-6.

Landis JR, Koch GG. The measurement of observer agreement for categorical data. *Biometrics.* 1977;33(1):159-74.

Lavini C. Simulating the effect of input errors on the accuracy of Tofts' pharmacokinetic model parameters. *Magn Reson Imaging.* 2015;33(2):222-35.

Leach MO, Morgan B, Padhani A, et al.; Experimental Cancer Medicine Centres Imaging Network Steering Committee. Imaging vascular function for early stage clinical trials using dynamic contrast-enhanced magnetic resonance imaging. *Eur Radiol.* 2012;22(7):1451-64.

Limkin EJ, Sun R, Fertié C, et al. Promises and challenges for the implementation of computational medical imaging (radiomics) in oncology. *Ann Oncol.* 2017;28(6):1191-1206.

Liu G, Rugo HS, Herbst RS, et al. Dynamic contrast-enhanced magnetic resonance imaging as a pharmacodynamic measure of response after acute dosing of AG-013736, an oral angiogenesis inhibitor, in patients with advanced solid tumors: results from a phase I study. *J Clin Oncol.* 2005;23(24):5464-73.

Lucas DR, Kshirsagar MP, Schuetze SM, et al. Histologic alterations from neoadjuvant chemotherapy in high-grade extremity soft tissue sarcoma: Clinicopathological correlation. *Oncologist* 2008;13:451-8.

Meyer JM, Perlewitz KS, Ryan CW, et al. Phase I trial of preoperative chemoradiation plus sorafenib for high-risk extremity soft tissue sarcomas with dynamic contrast-enhanced MRI correlates. *Clin Cancer Res.* 2013;19(24):6902-11.

Messiou C, Bonvalot S, Haas RL, et al.; European Organization for Research and Treatment of Cancer - Soft Tissue and Bone Sarcoma Group; European Organization for Research and Treatment of Cancer - Imaging Group. Evaluation of response after pre-operative radiotherapy in soft tissue sarcomas; the European Organisation for Research and Treatment of Cancer-Soft Tissue and Bone Sarcoma Group (EORTC-STBSG) and Imaging Group recommendations for radiological examination and reporting with an emphasis on magnetic resonance imaging. *Eur J Cancer.* 2016;56:37-44.

Monsky WL, Jin B, Chaudhari AJ, et al. Semi-automated volumetric quantification of tumor necrosis in soft tissue sarcoma using contrast-enhanced MRI. *Anticancer Res.* 2012;32(11):4951-61.

Morgan B, Thomas AL, Steward WP, et al. Dynamic contrast-enhanced magnetic resonance imaging as a biomarker for the pharmacological response of PTK787/ZK 222584, an inhibitor of the vascular endothelial growth factor receptor tyrosine kinases, in patients with advanced colorectal cancer and liver metastases: results from two phase I studies. *J Clin Oncol*. 2003;21(21):3955-64.

Mouridsen K, Christensen S, Gyldensted L, Ostergaard L. Automatic selection of arterial input function using cluster analysis. *Magn Reson Med*. 2006;55(3):524-31.

Padhani AR, Miles KA. Multiparametric imaging of tumor response to therapy. *Radiology*. 2010;256(2):348-64.

Partovi S, von Tengg-Kobligk H, Robbin MR, et al. Advanced Noncontrast MR Imaging in Musculoskeletal Radiology. *Radiol Clin North Am*. 2015;53(3):549-67.

Pasquali S, Palassini E, Gronchi A, et al. Neoadjuvant treatment: a novel standard? *Curr Opin Oncol*. 2017;29(4):253-259.

Perkins NJ, Schisterman EF. The inconsistency of "optimal" cutpoints obtained using two criteria based on the receiver operating characteristic curve. *Am J Epidemiol*. 2006;163(7):670-5.

Reddick WE, Bhargava R, Fletcher BD, et al. Dynamic contrast-enhanced MR imaging evaluation of osteosarcoma response to neoadjuvant chemotherapy. *J Magn Reson Imaging*. 1995;5(6):689-94.

Reichardt P, Lindner T, Dörken B, et al. Chemotherapy in alveolar soft part sarcomas. What do we know? *Eur J Cancer*. 2003;39(11):1511-6.

Rukat T, Walker-Samuel S, Reinsberg SA. Dynamic contrast-enhanced MRI in mice: an investigation of model parameter uncertainties. *Magn Reson Med*. 2015;73(5):1979-87.

Salzer-Kuntschik M, Delling G, Beron G, Sigmund R. Morphological grades of regression in osteosarcoma after polychemotherapy – study COSS 80. *J Cancer Res Clin Oncol* 1983;106:S21–4.

Saponara M, Stacchiotti S, Casali PG, Gronchi A. (Neo)adjuvant treatment in localised soft tissue sarcoma: The unsolved affair. *Eur J Cancer*. 2017;70:1-11.

Sanfilippo R, Casali PG. The intriguing patterns of tumor response to trabectedin. *Expert Rev Anticancer Ther*. 2013;13(6 Suppl 1):21-4.

Soldatos T, Ahlawat S, Fayad LM, et al. Multiparametric Assessment of Treatment Response in High-Grade Soft-Tissue Sarcomas with Anatomic and Functional MR Imaging Sequences. *Radiology*. 2016;278(3):831-40.

Stacchiotti S, Collini P, Casali PG, et al. High-grade soft-tissue sarcomas: tumor response assessment--pilot study to assess the correlation between radiologic and pathologic response by using RECIST and Choi criteria. *Radiology*. 2009;251(2):447-56.

Stacchiotti S, Verderio P, Gronchi A, et al. Tumor response assessment by modified Choi criteria in localized high-risk soft tissue sarcoma treated with chemotherapy. *Cancer*. 2012;118(23):5857-66.

Sullivan DC et al., Metrology standards for quantitative imaging biomarkers. *Radiology*. 2015;277:813-825.

Tofts PS, Brix G, Weisskoff RM, et al. Estimating kinetic parameters from dynamic contrast-enhanced T(1)-weighted MRI of a diffusable tracer: standardized quantities and symbols. *J Magn Reson Imaging*. 1999;10(3):223-32.

Trojani M, Contesso G, Lagarde C, et al. Soft-tissue sarcomas of adults; study of pathological prognostic variables and definition of a histopathological grading system. *Int J Cancer*. 1984;33(1):37-42.

Uhl M, Saueressig U, Langer M, et al. Osteosarcoma: preliminary results of in vivo assessment of tumor necrosis after chemotherapy with diffusion- and perfusion-weighted magnetic resonance imaging. *Invest Radiol.* 2006;41(8):618-23.

Van Rijswijk CS, Geirnaerd MJ, Bloem JL, et al. Dynamic contrast-enhanced MR imaging in monitoring response to isolated limb perfusion in high-grade soft tissue sarcoma: initial results. *Eur Radiol.* 2003;13(8):1849-58.

Van Rijswijk CS, Geirnaerd MJ, Bloem JL, et al. Soft-tissue tumors: value of static and dynamic gadopentetate dimeglumine-enhanced MR imaging in prediction of malignancy. *Radiology.* 2004;233(2):493-502.

Viglianti BL, Lora-Michiels M, Dewhirst MW, et al. Dynamic contrast-enhanced magnetic resonance imaging as a predictor of clinical outcome in canine spontaneous soft tissue sarcomas treated with thermoradiotherapy. *Clin Cancer Res.* 2009;15(15):4993-5001.

Wardelmann E, Haas RL, Bonvalot S, et al. Evaluation of response after neoadjuvant treatment in soft tissue sarcomas; the European Organization for Research and Treatment of Cancer-Soft Tissue and Bone Sarcoma Group (EORTC-STBSG) recommendations for pathological examination and reporting. *Eur J Cancer.* 2016;53:84-95.

White LM, Wunder JS, Kandel RA, et al. Histologic assessment of peritumoral edema in soft tissue sarcoma. *Int J Radiat Oncol Biol Phys.* 2005;61(5):1439-45.

Zhang X, Chen YL, El Fakhri G, et al. Synergistic role of simultaneous PET/MRI-MRS in soft tissue sarcoma metabolism imaging. *Magn Reson Imaging.* 2016;34(3):276-9.

SERMENT MEDICAL

Au moment d'être admise à exercer la médecine, je promets et je jure d'être fidèle aux lois de l'honneur et de la probité.

Mon premier souci sera de rétablir, de préserver ou de promouvoir la santé dans tous ses éléments, physiques et mentaux, individuels et sociaux.

Je respecterai toutes les personnes, leur autonomie et leur volonté, sans aucune discrimination selon leur état ou leurs convictions. J'interviendrai pour les protéger si elles sont affaiblies, vulnérables ou menacées dans leur intégrité ou leur dignité. Même sous la contrainte, je ne ferai pas usage de mes connaissances contre les lois de l'humanité.

J'informerai les patients des décisions envisagées, de leurs raisons et de leurs conséquences. Je ne tromperai jamais leur confiance et n'exploiterai pas le pouvoir hérité des circonstances pour forcer les consciences.

Je donnerai mes soins à l'indigent et à quiconque me les demandera. Je ne me laisserai pas influencer par la soif du gain ou la recherche de la gloire.

Admis(e) dans l'intimité des personnes, je tairai les secrets qui me seront confiés. Reçu(e) à l'intérieur des maisons, je respecterai les secrets des foyers et ma conduite ne servira pas à corrompre les mœurs.

Je ferai tout pour soulager les souffrances. Je ne prolongerai pas abusivement les agonies. Je ne provoquerai jamais la mort délibérément.

Je préserverai l'indépendance nécessaire à l'accomplissement de ma mission. Je n'entreprendrai rien qui dépasse mes compétences. Je les entretiendrai et les perfectionnerai pour assurer au mieux les services qui me seront demandés.

J'apporterai mon aide à mes confrères ainsi qu'à leurs familles dans l'adversité.

Que les hommes et mes confrères m'accordent leur estime si je suis fidèle à mes promesses ; que je sois déshonorée et méprisée si j'y manque.